NASA

COMMENTS ON THE SOLUTION OF THE SPALL-FRACTURE PROBLEM IN THE APPROXIMATION OF LINEAR ELASTICITY

by

William J. Rae

prepared for

NATIONAL AERONAUTICS AND SPACE ADMINISTRATION

CONTRACT NO. NAS 3-2536

CORNELL AERONAUTICAL LABORATORY, INC.
of Cornell University
Buffalo, New York 14221

GPO PRICE $ _____

OTS PRICE(S) $ _____

Hard copy (HC) $3.00

Microfiche (MF) $0.75

N65-19848

(ACCESSION NUMBER)

(PAGES)

CR-54250

(NASA CR OR TMX OR AD NUMBER)

(THRU)

(CODE)

32

(CATEGORY)

FACILITY FORM 602

NOTICE

This report was prepared as an account of Government sponsored work. Neither the United States, nor the National Aeronautics and Space Administration (NASA), nor any person acting on behalf of NASA:

A)   Makes any warranty or representation, expressed or implied, with respect to the accuracy, completeness, or usefulness of the information contained in this report, or that the use of any information, apparatus, method, or process disclosed in this report may not infringe privately owned rights; or

B)   Assumes any liabilities with respect to the use of, or for damages resulting from the use of any information, apparatus, method or process disclosed in this report.

As used above, "person acting on behalf of NASA" includes any employee or contractor of NASA, or employee of such contractor, to the extent that such employee or contractor of NASA, or employee of such contractor prepares, disseminates, or provides access to, any information pursuant to his employment or contract with NASA, or his employment with such contractor.

Requests for copies of this report should be referred to

    National Aeronautics and Space Administration
    Office of Scientific and Technical Information
    Attention: AFSS-A
    Washington, D. C.   20546

CASE FILE COPY

TOPICAL REPORT

COMMENTS ON THE SOLUTION OF THE SPALL-FRACTURE
PROBLEM IN THE APPROXIMATION OF LINEAR ELASTICITY

by

William J. Rae

prepared for

NATIONAL AERONAUTICS AND SPACE ADMINISTRATION

January 1965

CONTRACT NO. NAS 3-2536

Technical Management
NASA - Lewis Research Center
Space Electric Power Office
Martin Gutstein

CORNELL AERONAUTICAL LABORATORY, INC.
of Cornell University
Buffalo, New York   14221

FOREWORD

This document describes a portion of the research conducted in a study of the application of the blast-wave theory of meteoroid impact to the problem of space radiator design. Other publications generated under this NASA-sponsored program include "Nonsimilar Solutions for Impact-Generated Shock Propagation in Solids, "CAL Report AI-1821-A-2, NASA CR-54251, January 1965, and "On the Possibility of Simulating Meteoroid Impact by the Use of Lasers, "CAL Report AI-1821-A-1, NASA CR-54029, April 1964.

ABSTRACT 19848

This report presents a study of the tensile stresses produced when a compressive spherical wave is reflected from a plane, stress-free surface. Two classes of exact solution of the problem, within the approximation of linear elasticity, are reviewed. In one class, the incident stress distribution is spherically symmetric, while in the other it is only axisymmetric, allowing a variation in one angular coordinate. A significant difference exists between the two classes in the laws relating the strength of incident and reflected waves. The implications of this difference on the reflection of impact-generated stress waves are discussed.

The exact solution for cases where the incident wave exhibits spherical symmetry is examined in detail, and simple quadrature formulas for obtaining the reflected stress profile for a given incident waveform are presented. These results are compared with the commonly used solution which considers only the stresses due to a source and its image. The conditions under which this further approximation is acceptable are discussed.

The limitations of a linear elastic model in predicting spall fracture are pointed out, and the areas most in need of further study are indicated.

AuTHOR

TABLE OF CONTENTS

AI-1821-A-3

LIST OF SYMBOLS

a in Sec. IV, the radius of application of pressure P - see Eq. (20); in Sec. V, function defined in Eq. (65)

a_1, b_1 constants defined in Eq. (11)

b function defined in Eq. (65)

A, B in Sec. IV, functions defined in Eq. (34); in Sec. V, functions defined in Eq. (61)

$A_3(\tau)$ function defined in Eq. (64)

c weak-wave speed in linear shock-speed, particle-speed relation, see Eq. (1)

c_1 dilatational wave speed, $\sqrt{\dfrac{\lambda + 2\mu}{\rho_0}}$

c_2 shear wave speed, $\sqrt{\dfrac{\mu}{\rho_0}}$

D function defined in Eq. (65)

$\mathcal{D}, \mathcal{D}'$ functions defined in Eq. (76)

E projectile kinetic energy

F displacement potential, Secs. II and V; magnitude of point force, Sec. IV

$F_{1,2,3}$ functions defined in Eq. (47)

$\mathcal{G}$ function defined in Eq. (105)

g $= c_1/c_2$

$g_{1,2,3}$ functions defined in Eqs. (49 - 51)

h target thickness

$H(\theta_2)$ function defined in Eq. (16)

i $\sqrt{-1}$

$I_{1,2}$ angles defined in Eq. (58)

$N_{1,2}$ functions defined in Eq. (27)

p	pressure; also Laplace transform variable
P	magnitude of applied pressure - see Eqs. (20) and (21)
q	$= 1/g$
$Q_{0,1,2}$	functions defined in Eq. (23)
r, z, φ	cylindrical coordinates
R, θ	spherical coordinates
R_c	cavity radius
R_s	shock radius
R_o	$= \left(E / 2\pi \rho_o c^2 \right)^{1/3}$
R_1, R_2	in Sec. III, distances defined in the sketch accompanying Eq. (16); in Sec. V, distances defined in Eq. (58)
R, R'	distances defined in the sketch preceding Eq. (58) and in Eq. (87)
s	in Sec. II, constant in the linear shock-speed, particle-speed relation, see Eq. (1); elsewhere, $s = 1/c_2$
S	$= 1/c_1$
t	time
u_s, u_1	shock speed, particle speed, Eq. (1)
u	variable defined in Eq. (64)
u, v	displacements in the r and z directions
U	displacement in the R direction
$v_{1,2,3}$	functions defined in Eq. (101)
$V_{1,2,3}$	functions defined in Eq. (76)
V	$= V_1 + V_2 + V_3$
x	variable defined in Eqs. (76) and (81)
α, β	in Sec. IV, functions defined in Eq. (28); in Sec. V, functions defined in Eq. (76)

ζ function defined in Eq. (79)

$\eta(t)$ variable defined by one of Eqs. (41 - 43)

$\theta_{1,2}$ angles defined in sketch accompanying Eq. (16)

λ, μ Lamé constants

ν Poisson's ratio, $\nu = \dfrac{\lambda}{2(\lambda + \mu)}$

ξ variable defined in Eq. (11)

ρ_0 target density

σ normal stress

σ_m mean stress

τ shear stress; also used as a dummy variable; also as a time
variable in Sec. V, see Eqs. (69), (74), and (81)

ϕ, Φ, ψ displacement potentials, see Eq. (7)

$(\ )_{P,S,PP,PS}$ denotes conditions, respectively, along the incident dilatational
wave, incident shear wave, dilatational and shear waves generated
by first reflection of incident dilatational wave

$\mathcal{R}e, \mathcal{I}m$ denotes real or imaginary part

I. INTRODUCTION

The impact of fast-moving particles drives strong compression waves into a solid body. When such waves arrive at a stress-free surface, they are reflected as tensile waves. Depending on the intensity and waveform of the incident pulse, the tensile stresses generated upon reflection may cause a fracture near the free surface, a process referred to as spallation. Damage of this sort can be a source of great concern in certain situations, for example in the case of space radiator systems.[2]

A precise theoretical treatment of the spallation problem is made difficult by the fact that different equations apply during successive stages of the deformation. In the early stages, for example, the compression consists of a strong shock wave, whose motion through the solid is described by the equations of a compressible, inviscid fluid. The shock decays as it propagates into the target, and the material strength then begins to play a role. During this stage, plastic deformation predominates for a while, and ultimately the entire process becomes elastic.

Many approximations have been proposed for treating this problem. One of the simplest of these* is to use the inviscid, compressible-fluid description up to the point where the incident wave first reaches the free surface. From that instant on, the motion is assumed to be described by the classical equations of linear elasticity, using the pressure distribution behind the shock to give the incident compressive stress distribution. The entire problem is then reduced to the simple question: What tensile stresses are developed along the axis of symmetry when a given compressive stress wave reflects from a plane, stress-free boundary?

---

*See, for example, Ref. 3, Appendix A.

The fact is that this question has never been thoroughly examined, although the needed results are contained in a number of papers, particularly from the field of seismology. The principal objective of this report is to extract these results in a form particularly suited to the spallation problem, using them to evaluate further approximations that can be used, and to shed light on the effects of various parameters.

The approximation in which the spall-fracture problem is to be treated in this report is formulated in Section II. A brief review is given there of the present state of knowledge of the stress distributions that are generated in hypervelocity impact. With the incident distribution considered to be a specified function, the question of its reflection from a free surface is then posed in the linear elastic approximation.

Solution of the specified elastic problem begins in Section III with a review of a method of solution which uses a pressurized cavity as the source of the spherical disturbance, together with an image system to preserve the boundary conditions at the free surface. The contributions arising from various portions of the image system are presented in detail, in order to assess their relative importance. It is shown that, for incident stress profiles which rise instantaneously to a maximum and then decay rapidly, the maximum tensile stress at the front of the reflected wave can be adequately calculated by the approximation that considers only the source cavity and an image cavity experiencing the same pressure, but with opposite sign.

In Section IV, a second class of solution is considered, in which the incident wave is generated by the application of a point force to one free surface of a slab. The wave that results is spherical in shape, but displays an angular variation not present in the spherically symmetric solution. This

angular variation gives rise to an increase in the amplitude of the reflected wave.

Section V returns to a consideration of the spherically symmetric case, and the solution for a point source and its image system is cast in the form of a quadrature formula from which the reflected stress profile can be calculated, once the incident profile is known.

The report concludes with a discussion of the areas where deficiencies still exist in the linear-elastic treatment of the problem, and mention is made of the most important areas in which improvement over such a model should be sought. Finally, the implications of these studies on the interpretation of spall-fracture experiments are pointed out.

II. STATEMENT OF THE PROBLEM

General Considerations

When a projectile strikes a solid target at high speed, a shock wave is generated which becomes approximately spherical in shape after a period several times that required for the projectile to travel its own length.[4] The shock decays in strength as it propagates through the target and ultimately degenerates to an elastic wave. If it encounters a stress-free surface, it is reflected as a tensile wave, whose amplitude may be sufficient to cause a spall fracture. The fundamental problem is to determine what target thickness is required to prevent such a fracture, when the projectile mass and velocity are specified.

If the target is sufficiently thin, or the impact speed sufficiently high, the reflection will take place in a region where the target is incapable of sustaining tensile stress, and a puncture results. At the other extreme, where the target is sufficiently thick in relation to the severity of the impact, the reflection will follow the classical equations of elasticity. In the intermediate regime, the plastic and viscoelastic behavior of the target play a role.

A rigorous theoretical treatment of such a complex problem, valid for all regimes, is obviously quite difficult. This report presents an approximate treatment in which the plastic regime is ignored entirely; instead, the target is assumed to behave like a compressible, inviscid fluid up to the instant when the shock reaches the free surface; thereafter, the classical equations of linear elasticity are assumed to apply, with the incident stress distribution given in terms of the pressure distribution behind the incident shock. This approximation has been proposed before;[3] the purpose of this report is to examine its predictions more fully.

AI-1821-A-3

It should be emphasized that the problem, when formulated this way, is capable of solution without regard to the specific details of the incident waveform. As is typical of linear problems, it is possible to identify an indicial response; the solution for a specific excitation is then expressed as a convolution of the incident profile with this indicial response.

Incident-Wave Profile

A considerable amount of information is now available concerning the early period of deformation, during which the target deforms as a compressible, inviscid fluid. Numerical solutions of the equations appropriate to this regime were first reported by Bjork,[5,6] who used the particle-in-cell method to obtain results in aluminum, iron, and tuff. More recently, Walsh[4,7] made use of both a particle-in-cell and an Eulerian computer code to produce results with greatly improved resolution for an expanded list of materials, including lead and polyethylene plastic. Parallel developments based on blast-wave theory[8-11] have provided useful approximations. Many of these analytical developments are summarized in Ref. 1.

A typical representation of the pressure distribution along the axis of symmetry is shown in Fig. 1. The coordinate system used is a cylindrical one, with origin at the impact point on the front face of the target.
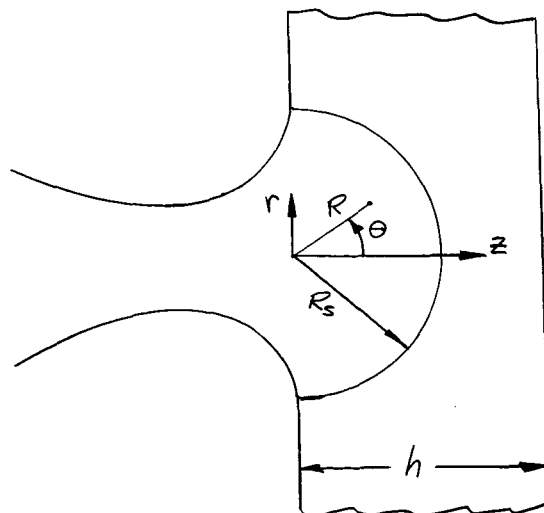
The target thickness is denoted by h , while R_s , a function of time, represents the (spherical) radius of the shock at any instant.

The curves of Fig. 1, taken from Ref. 1, are based on the approximation that the flow can be represented as one half of a spherically symmetric disturbance. Such a flow is sensitive only to the total energy available; its momentum is zero by symmetry. Thus, as in all explosion problems,[12] the natural scale of distance in the problem, R_o , is proportional to the cube root of the energy release divided by the characteristic pressure in the medium. It was shown in Ref. 9 that this pressure is given by $\rho_o c^2$, where ρ_o is the target density under normal conditions, and c is the weak-wave velocity appearing in the linear shock speed-particle speed relation

$$u_s = c + s u_1 \tag{1}$$

For most materials, the value of c is approximately equal to the bulk dilatational wave velocity.[13] Typical values of s lie in the range from 1 to 2.

It should be emphasized that the curves of Fig. 1 are intended only to convey a general impression of the disturbance generated by impact. Their quantitative significance is limited by the approximations on which they are based. For example, the stress distributions generated by an actual impact are not spherically symmetric; for $\theta \neq 0$, the pressure distribution would differ somewhat from that shown in Fig. 1. Furthermore, scaling with respect to energy alone is not exactly correct, as Walsh and his co-workers have shown.[4,7]

The general nature of the pressure distribution reveals a discontinuous jump at the wave, followed by a relatively steep decay. These features have also been observed in the results of Allen and Goldsmith,[14] who calculated the stress waves generated by applying, to the interior of a spherical cavity in an infinite medium, a pressure that rises instantaneously to a maximum, and then decays exponentially.

Conversion to Incident Stress Profile

In the present approximation, the material response is assumed to become elastic at the instant when the incident wave reaches the rear surface $z = h$. With such an approximation, the basic differential equations describing the motion become linear. Thus it is unnecessary to be specific about the waveform of the incident pulse. It is sufficient to find the solution for a step-function; results for an arbitrary waveform may then be found from a Duhamel integral. Nonetheless, it is instructive to indicate one method by which the incident waveform might be specified.

For example, the incident stress distribution can be calculated by equating the pressure p from the fluid-mechanical theory to the mean stress σ_m . Allen and Goldsmith have pointed out[14] that the product σ times the spherical radius R satisfies the plane-wave equation, i. e. ,

$$-p = \sigma_m = \left(\lambda + \frac{2}{3} \mu \right) \frac{F''\left(t - R/c_1 \right)}{c_1^2 R} \qquad (2)$$

where λ and μ are Lamé constants, t the time, $F(t)$ the value of the displacement potential at $R = 0$, and c_1 is the dilatational wave speed

$$c_1^2 = \frac{\lambda + 2\mu}{\rho_o} \qquad (3)$$

Thus, specification of the pressure versus distance at a given time t_1 is equivalent to specifying σ_m at a time, for the stress-wave analysis, given by $t = R_s(t_1)/c_1$.
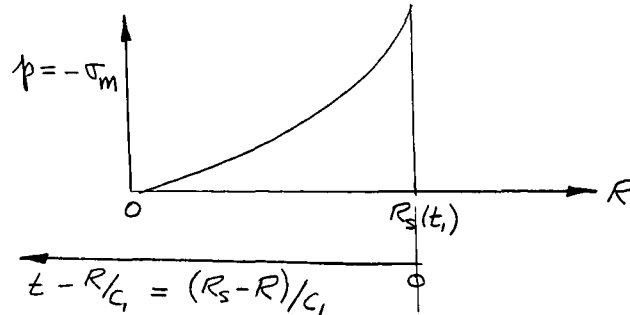
Once the function F is known, it can be used to find the other stress components; for example

$$\sigma_z = \frac{4\mu\, F\left(t - R/c_1\right)}{R^3} + \frac{4\mu F'\left(t - R/c_1\right)}{c_1 R^2} + \frac{(\lambda + 2\mu)\, F''\left(t - R/c_1\right)}{c_1^2 R} \qquad (4)$$

Knowledge of the function F over a given range of R at one instant is equivalent to knowing it over a displaced range at a later instant, since it depends only on the characteristic coordinate $t - R/c_1$:
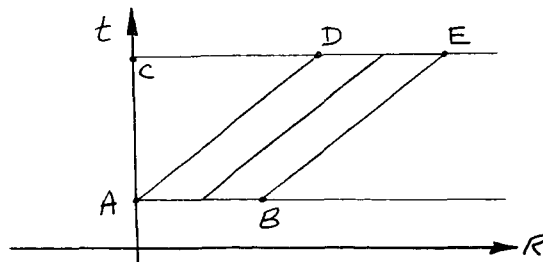

Thus, known conditions along AB are sufficient to determine conditions along DE . To find out about the range CD , it is necessary to know what was happening at $R = 0$ during the time interval AC .

For incident waves which lack spherical symmetry, the above considerations do not apply, and a more elaborate description of conditions behind the incident wave is necessary.

AI-1821-A-3

Simple Reflection Formulas

Much of our present understanding of the mechanism of spall fracture has come from consideration of the plane-wave case (see, for example, the treatment by Rinehart and Pearson in Ref. 15). In that case, the exact solution of the equations of elasticity reveals that the reflected wave is the inverted image of the incident wave:
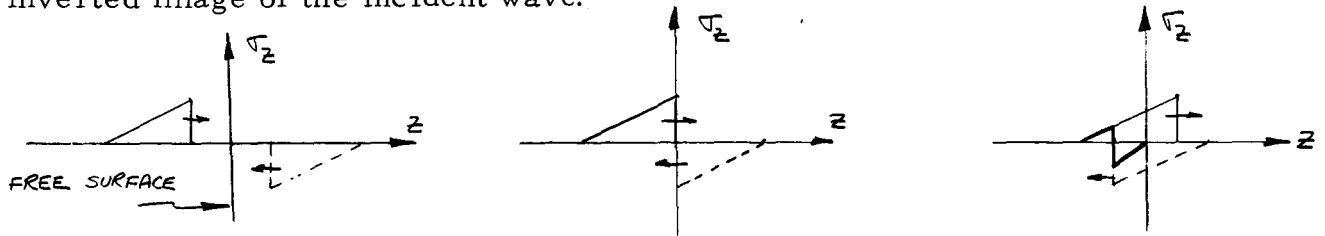
A simple extension of this solution to the spherical case is to assume that the solution is still given by the sum of the incident wave and its inverted image, allowing both contributions to decay with distance the way they would in an infinite medium:
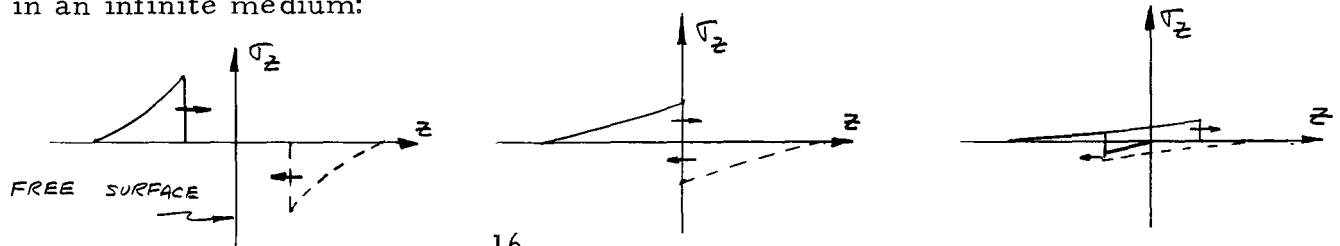
It has been pointed out before[16] that such a construction is not an exact solution of the problem. One of the objectives of the present report is to determine how good the approximation is.

III. WAVES DUE TO A SPHERICAL CAVITY

One means of studying the reflection of spherical stress waves is to examine the disturbance produced by applying a pressure to the interior of a spherical cavity in the medium.   The waves that result have spherical symmetry, and their reflection at a free surface has been considered in recent papers by Aliev[17] and by Kinslow.[18] This section presents a review of their work, noting the physical significance of the various contributions to the solution.

Basic Relations

The cavity, of radius R_c , is located with its center a distance h from the free surface.   Cylindrical coordinates r and z , and spherical radius R are measured from the center of the cavity
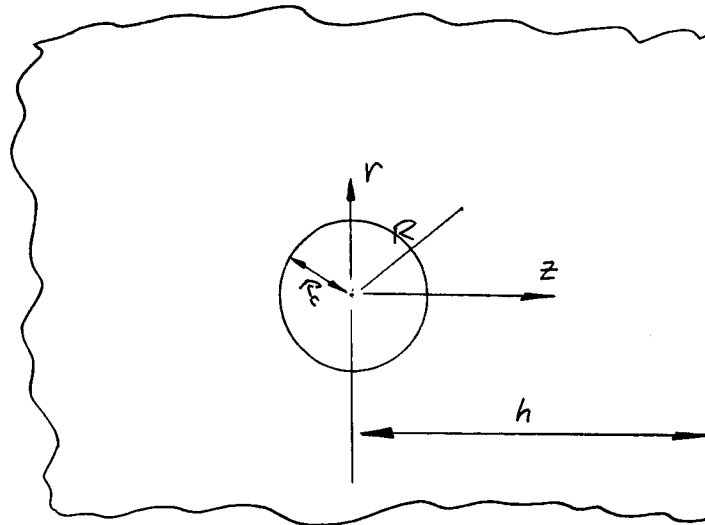
Displacements in the r , z and R directions are denoted by u , v and U , respectively. In terms of these displacements, the normal stresses σ and shear stresses τ are given by

$$\sigma_r = \lambda \left(\frac{\partial u}{\partial r} + \frac{\partial v}{\partial z} + \frac{u}{r} \right) + 2\mu \frac{\partial u}{\partial r}$$

$$\sigma_z = \lambda \left(\frac{\partial u}{\partial r} + \frac{\partial v}{\partial z} + \frac{u}{r} \right) + 2\mu \frac{\partial v}{\partial z}$$

$$\sigma_\varphi = \lambda \left(\frac{\partial u}{\partial r} + \frac{\partial v}{\partial z} + \frac{u}{r} \right) + 2\mu \frac{u}{r}$$

$$\tau_{rz} = \mu \left(\frac{\partial u}{\partial z} + \frac{\partial v}{\partial r} \right) \quad ; \quad \tau_{r\varphi} = \tau_{\varphi z} = 0 \tag{5}$$

$$\sigma_R = (\lambda + 2\mu) \frac{\partial U}{\partial R} + 2\lambda \frac{U}{R}$$

$$\sigma_\theta = \lambda \frac{\partial U}{\partial R} + 2(\lambda + \mu) \frac{U}{R}$$

while the equations of motion take the form

$$\frac{\partial \sigma_r}{\partial r} + \frac{\partial \tau_{rz}}{\partial z} + \frac{\sigma_r - \sigma_\varphi}{r} = \rho_0 \frac{\partial^2 u}{\partial t^2}$$

$$\frac{\partial \tau_{rz}}{\partial r} + \frac{\partial \sigma_z}{\partial z} + \frac{\tau_{rz}}{r} = \rho_0 \frac{\partial^2 v}{\partial t^2} \tag{6}$$

$$\frac{\partial \sigma_R}{\partial R} + \frac{2}{R} (\sigma_R - \sigma_\theta) = \rho_0 \frac{\partial^2 U}{\partial t^2}$$

These equations can be decoupled by use of the displacement potentials ϕ, ψ, and Φ, defined by

$$u = \frac{\partial \phi}{\partial r} - \frac{\partial \psi}{\partial z} \quad ; \quad v = \frac{\partial \phi}{\partial z} + \frac{\partial \psi}{\partial r} + \frac{\psi}{r} \quad ; \quad U = \frac{\partial \Phi}{\partial R} \tag{7}$$

11   AI-1821-A-3

The equations that result are

$$c_1^2 \left(\frac{\partial^2 \phi}{\partial r^2} + \frac{\partial^2 \phi}{\partial z^2} + \frac{1}{r} \frac{\partial \phi}{\partial r} \right) = \frac{\partial^2 \phi}{\partial t^2}$$

$$c_2^2 \left(\frac{\partial^2 \psi}{\partial r^2} + \frac{\partial^2 \psi}{\partial z^2} + \frac{1}{r} \frac{\partial \psi}{\partial r} - \frac{\psi}{r^2} \right) = \frac{\partial^2 \psi}{\partial t^2} \tag{8}$$

$$c_1^2 \left(\frac{\partial^2 \Phi}{\partial R^2} + \frac{2}{R} \frac{\partial \Phi}{\partial R} \right) = \frac{\partial^2 \Phi}{\partial t^2}$$

where $c_2^2 = \mu / \rho_0$.

Source Solution

The solution for the case where the cavity experiences a pressure

$$\sigma_R \Big)_{R=R_c} = \begin{cases} 0, & t < 0 \\ -p(t), & t > 0 \end{cases} \tag{9}$$

has been given by Blake,[19] and others. It can be written in the form

$$\Phi(t, R) = + \frac{\rho_0 R_c}{c_1^2 b_1 R} \int_0^\xi p\left(\frac{x}{c_1}\right) \exp\left[a_1(x-\xi)\right] \sin\left[b_1(x-\xi)\right] dx \tag{10}$$

where

$$a_1 = \frac{2}{R_c g^2} \quad , \quad b_1 = \frac{2\sqrt{g^2-1}}{R_c g^2} \quad , \quad g^2 = \frac{c_1^2}{c_2^2} = \frac{\lambda + 2\mu}{\mu} = \frac{2(1-\nu)}{1-2\nu} \tag{11}$$

$$\xi = c_1 t - R + R_c$$

and where Poisson's ratio is denoted by ν . Complete expressions for

the displacements and stresses have been presented by Blake,[19] by Aliev[17]

and by Allen and Goldsmith,[14] who present detailed results for the case

where $p(t) = p_0 e^{-kt}$.

Image System

In order to find how this disturbance is reflected from the free surface, one is led to consider the effect of a second spherical cavity, also of radius R_c, and located at $z = 2h$. Aliev makes use of such an image, allowing it to experience the same pressure as the cavity at $z = 0$. The result is to produce zero shear stress at the free surface, but a non-zero normal stress σ_z. If, on the other hand, the image cavity experiences the same pressure as the original one, but with opposite sign, the stress σ_z is made zero at the free surface, but a net shear stress τ_{rz} is developed. In either case, the cavity at $z = 2h$ is not enough; the complete image system must include a second contribution distributed along the free surface in such a way as to cancel the nonzero stress due to the two cavities. [*]

The stress components arising from the two cavities can be visualized by considering a spherical displacement which decays with R, corresponding to a compression


---
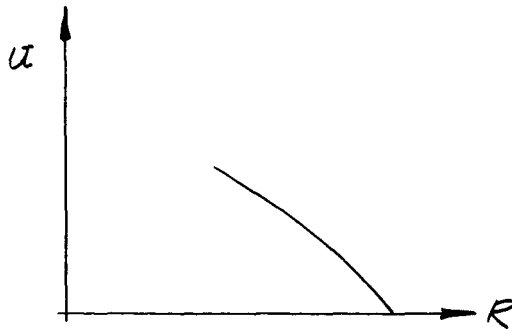
[*] Professor Norman Davids of the Pennsylvania State University has pointed out to the author in a private communication (April 23, 1964) that the same conclusion can be reached simply by considering a source potential $\phi = r^{-1} f(r - c_1 t)$, and an image potential $\phi = -r^{-1} f(r + c_1 t)$. The author is very grateful to Professor Davids for a very informative discussion of this problem.

For the case where a compression is applied to both cavities (as Aliev does), this sketch of U versus R can be used to construct the displacements at four points (all having different values of R) near the free surface. The displacements have the appearance
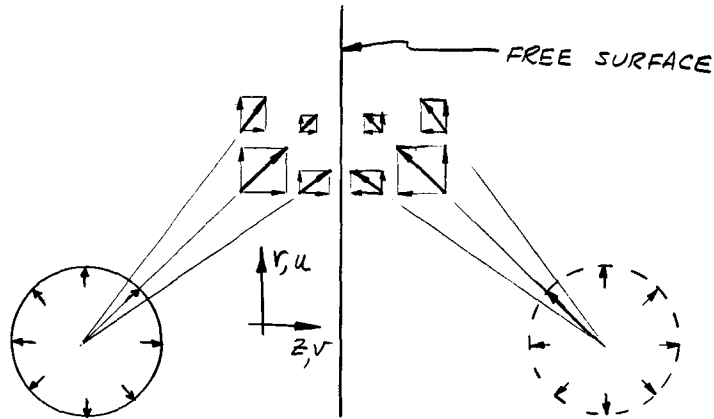

From this sketch it can be seen that the displacement gradients are as follows
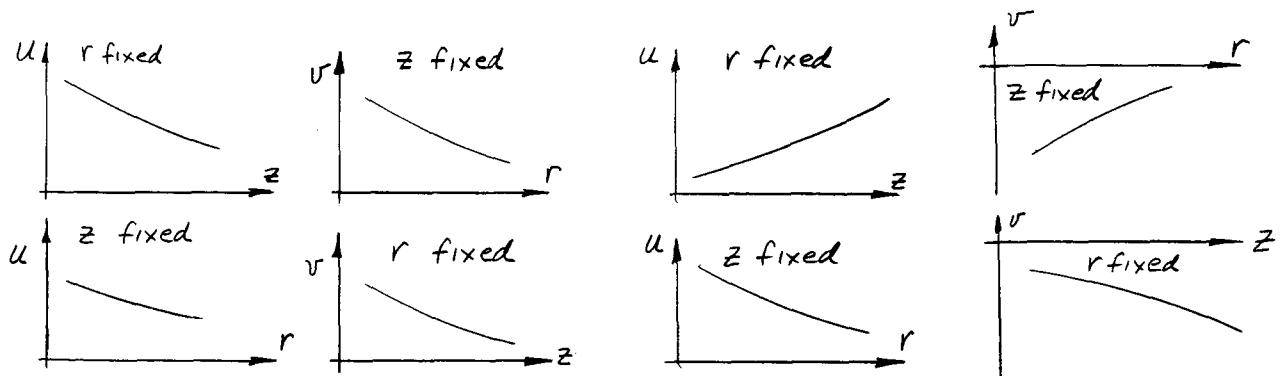
Note that, at the interface, the contributions to $\left(\frac{\partial u}{\partial z}\right)_r$ and to $\left(\frac{\partial v}{\partial r}\right)_z$ coming from the two cavities are of opposite sign, while the contributions to $\left(\frac{\partial u}{\partial r}\right)_z$ and $\left(\frac{\partial v}{\partial z}\right)_r$ are of the same sign. Thus the net effect of two compressive cavities is to produce zero shear stress τ_{rz} at the surface, but a nonzero normal stress σ_z .
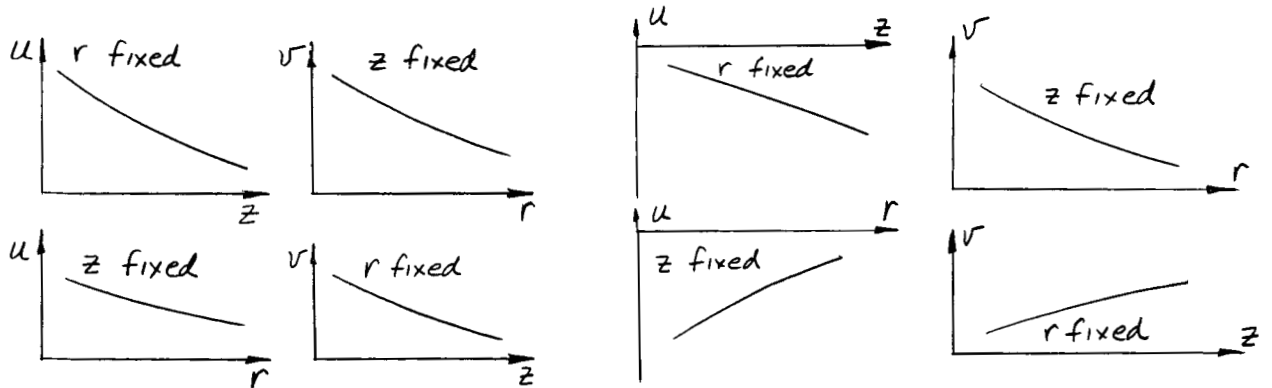
On the other hand, if a tensile stress is applied to the interior of the image cavity, so that it generates displacements which increase with R
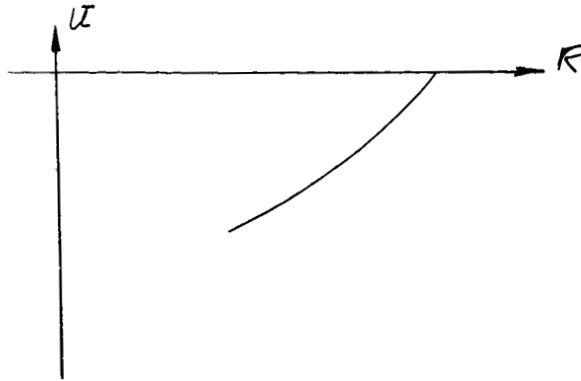
the resultant displacements have the appearance
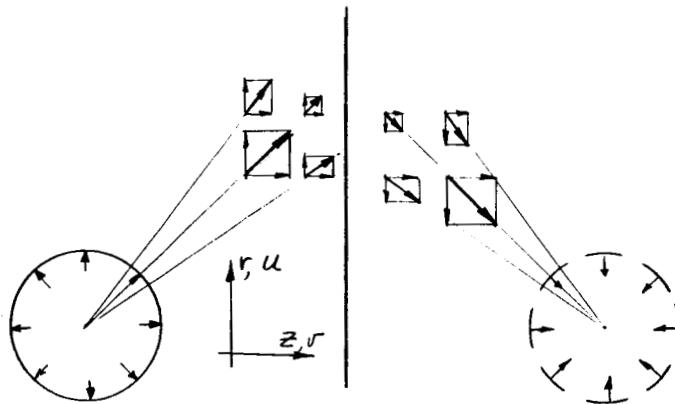
and the associated gradients are as follows

In this case, the contributions to u, $\left(\partial u/\partial r\right)_z$ and $\left(\partial v/\partial z\right)_r$ are of oppo-
site sign and cancel, while the contributions to $\left(\partial u/\partial z\right)_r$ and $\left(\partial v/\partial r\right)_z$
add. Thus there is no normal stress σ_z at the free surface, but a net
shear stress τ_{rz} is developed, whose sign is negative

AI-1821-A-3
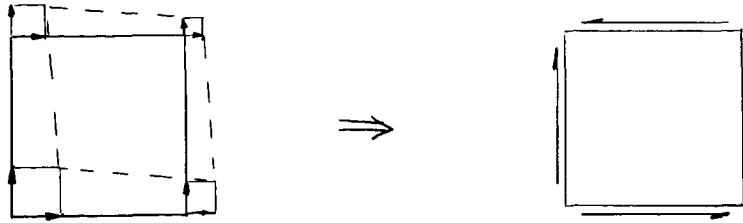
In addition to the image cavity, then, the complete solution requires the application of a positive distribution of τ_{rz} on the free surface.

Effect of the Surface Distribution

As mentioned earlier, the approximation is often made that the surface-distributed shear stresses can be neglected, and that only the compressive source cavity and tensile image cavity need to be considered. Kinslow's work, [18] for example, is based on this approximation. To estimate the accuracy of the approximation, it is necessary to determine the size of the contribution from the surface stresses. An answer can be found by making a slight modification of Aliev's results, since the solution for a compressive source and tensile image can be found merely by changing, in Aliev's work, the sign of the displacements due to the image (for example, the sign of f_z in Aliev's Eqn. 2.4 is reversed). For the case where the source cavity experiences a step-function pressure

$$p = \begin{cases} 0 \,, & t < 0 \\ p_0, & t > 0 \end{cases} \qquad (12)$$

the resulting shear stress produced at the surface is given by

AI-1821-A-3

$$\frac{\tau_{rz})_{z=h}}{p_o} = \frac{\mu}{\rho_o c_1^2}\left[4\sin\theta_1\cos\theta_1\left\{\frac{R_c}{R}e^{-a_1\xi}\left(\frac{q}{\sqrt{q^2-1}}\sin b_1\xi - \cos b_1\xi\right)\right.\right.$$

$$\left.\left. -3\left(\frac{R_c}{R}\right)^2\frac{q^2 e^{-a_1\xi}\sin b_1\xi}{2\sqrt{q^2-1}} - \frac{3q^2}{4}\left(\frac{R_c}{R}\right)^3\left[1 - e^{-a_1\xi}\left(\frac{q}{\sqrt{q^2-1}}\sin b_1\xi + \cos b_1\xi\right)\right]\right\}\right] \tag{13}$$

The angle θ_1 is defined as $\cos^{-1}\frac{r}{R}$, as shown below
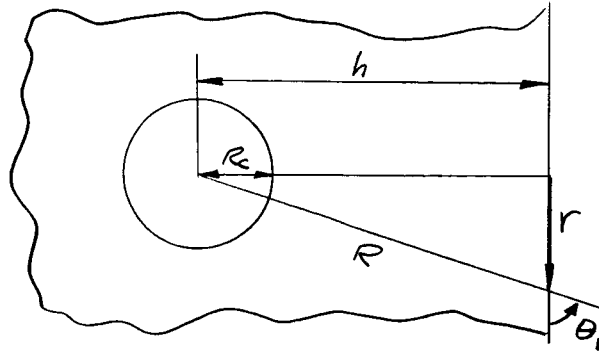
and a_1 and b_1 are defined as before, so that

$$a_1\xi = \frac{2}{q^2}\left(\frac{c_1 t}{R_c} - \frac{R}{R_c} + 1\right) \qquad b_1\xi = \frac{2\sqrt{q^2-1}}{q^2}\left(\frac{c_1 t}{R_c} - \frac{R}{R_c} + 1\right) \tag{14}$$

These results are shown in Fig. 2 for the case $\frac{h}{R_c} = 3$, $\nu = \frac{1}{4}$.

As noted above, the shear stress produced by the two cavities is negative; to cancel it, a positive stress of the same magnitude must be added, resulting in stresses within the target, in addition to those generated by the cavities. In assessing the magnitude of this contribution, two facts are important. The first is that $\tau_{rz})_{z=h}$ is of the order of p_o, i.e., it is generally of the same order as the stresses produced by the cavities. On the other hand, it is significant to note that the additional applied stress is zero at $r = 0$; thus, according to ray-theory,[20] it will make no contribution along the axis at the front of the reflected wave. The

same conclusion is derived below in Section V for the case of a point-source disturbance, namely, that for incident waves having spherical symmetry, the tensile stress developed at the front of the reflected dilatational wave, along the axis of symmetry, is exactly that given by the source and its image. Behind the front, the simple solution is no longer correct, but even there the approximation will be shown (in Section V) to be acceptable provided the stress amplitude decays rapidly enough behind the incident wave.

Off-Axis Conditions

At points located off the axis of symmetry, but on the reflected dilatational wave front, the effect of the surface stresses is compressive. Thus the source-plus-image approximation will overestimate the tensile stress at these points. This conclusion can be discerned in Aliev's results. After identifying the surface stresses that must be added, he approximates their effect by ray theory, using for this purpose the results of Bagdoev, a summary of which has recently appeared in translation.[21] Aliev's result is that the jump is stress $\left[\sigma_z \right]$ across the reflected dilatational wave is given by
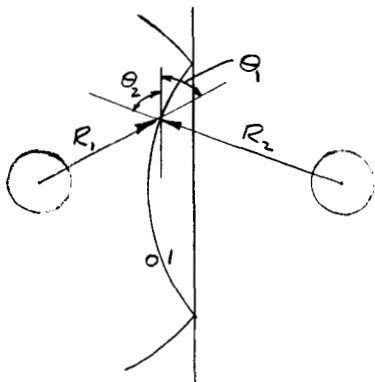
$$\left[\sigma_z \right] \equiv \left. \sigma_z \right)_1 - \left. \sigma_z \right)_0 = p_0 \frac{R_c}{R_2} \left[1 - \frac{2 \cos^2 \theta_2}{q^2} \right] \left[1 - \frac{2H}{1+H} \right] \quad (15)$$

$$H(\theta_2) = \frac{4 \sin \theta_2 \cos^2 \theta_2 \sqrt{1 - \frac{\cos^2 \theta_2}{q^2}}}{q^3 \left[1 - \frac{2 \cos^2 \theta_2}{q^2} \right]^2} \quad (16)$$

where R_2 and θ_2 are defined in the sketch above, and p_0 is the value of the pressure in the source cavity at $t = 0^+$. Figure 3 shows the varia-

tion of H with θ_2 for $\nu = 1/4$. The leading term (unity) in the last bracket of Eq. (15) represents the tensile jump, due only to the source and image. The next term, involving H , is of opposite sign, representing a compressive effect.

Thus it appears that, for incident waves having spherical symmetry, the source-image construction is exact at the front of the reflected wave, along the axis of symmetry, where the maximum tensile stress is likely to be developed. For points off the axis of symmetry, a more exact solution would add a compressive contribution, while at points on the axis of symmetry behind the reflected dilatational wave, the considerations given in Section V suggest that a more exact solution does not alter the maximum tensile stress, at least for incident wave forms which decay rapidly.

Kinslow's Work

The above conclusions are of importance in interpreting the work of Kinslow,[18] who makes use of the source-image approximation, applying it to incident waves which are finite sums of the Blake-type[19] solution. The pressure in the source cavity is taken to be

$$\frac{p}{p_1} = K_1 e^{-\alpha t} + K_2 e^{-2\alpha t} + \cdots + K_n e^{-n\alpha t} \qquad (17)$$

Actually, because of the conditions applied to find the coefficients K_i (all derivatives of p , beginning with the first and ending with the $(n-1)st$, are set equal to zero at $t = 0$), Eq. (17) becomes a binomial series, which can be summed as

$$\frac{p}{p_1} = 1 - \left(1 - e^{-\alpha t}\right)^n \qquad (18)$$

Kinslow presents results for selected values of α and n , evaluating p_1 from the formula

$$p_1 = \frac{\rho_o c r v}{r_1}$$

(19)

where c is the target stress-wave speed, r_1 , the radius of the crater that would be produced in an infinite target, r the depth of the free surface, and v the particle velocity behind the incident shock when it reaches the free surface.
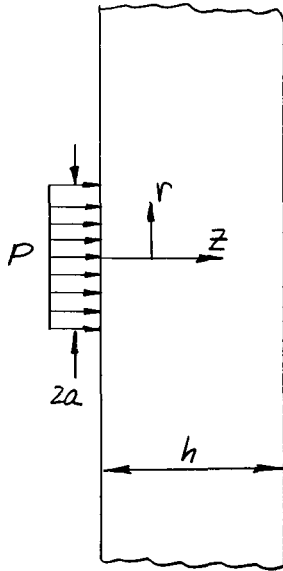
IV. WAVES DUE TO A POINT FORCE

A second means of representing incident stress waves like those encountered in hypervelocity impact is to consider the application of a force to one side of a slab of finite thickness. The solution for the disturbance which propagates into a slab due to the application of a distributed force has been presented by Huth and Cole,[22] and by Thiruvenkatachar.[23] The solution describing the reflection of these waves by a second free surface has been given by Thiruvenkatachar.[24] The waves induced by application of a point force, and their subsequent reflection, are discussed by Broberg,[25] and by Davids.[26]

A point force generates a wave whose shape is spherical, but the stress distribution behind it is not spherically symmetric. Furthermore, an incident shear wave is generated; no such feature appears in the solutions of the previous section.

The most distinctive feature of the solutions discussed below is that the laws relating the strengths of incident and reflected waves differ considerably from those that apply for spherically symmetric waves. The main purpose of this section is to discuss this feature.

Distributed, Step-Function Load

It is instructive to start from the solution for a step-function pressure applied over a circle of radius a

$$\tau_{rz} = 0 \quad , \quad z = 0 \, , \, z = h$$

$$\sigma_z = 0 \quad , \quad z = h \tag{20}$$

$$\sigma_z = \left\{ \begin{array}{l} 0 \quad , \quad r > a \\ \\ P1(t) \, , \, r < a \end{array} \right\} \, , \quad z = 0$$

The case treated by Thiruvenkatachar[23, 24] makes use of a delta function instead of the unit step $1(t)$. The problem solved by Davids is that of a point force F applied at $r = 0$. Thus it should be possible to recover the latter results by taking the limit $a \to 0$, $P \to \infty$, in such a way that

$$\pi a^2 P = F \tag{21}$$

Both of these authors employ the Laplace transform to derive formal expressions for the transforms of the various stress components. These expressions are then expanded in series whose successive terms represent the incident, reflected, and multiply reflected waves. For example, it is possible to sketch the progress of the various waves along the axis $r = 0$ in a z, t diagram
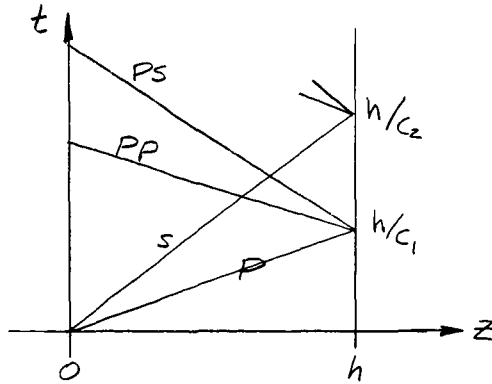
In the analysis that follows, only the incident dilatational (P) wave, and the reflected dilatational (PP) and shear (PS) waves are accounted for. Thus the results given below give no information about the state of affairs that exists after passage of the incident shear (S) wave.[*]

The Laplace transform of the solution for an applied pressure $P1(t)$ can be found by replacing P , wherever it occurs in Thiruvenkatachar's analysis, by P/p , where p denotes the transform variable

$$\bar{f}(p) = \int_0^\infty f(t)\, e^{-pt}\, dt \tag{22}$$

With this replacement, the transform of the stress component σ_z , in the region affected only by the incident dilatational wave, and the reflected dilatational and shear waves (i. e. , the triangle, in the sketch above, bounded by the lines $t = 0$, $z = h$, $t = z/c_2$) is[24]

$$\bar{\sigma}_z = \frac{aP}{p}\left\{ \bar{Q}_0 + \bar{Q}_1 + \bar{Q}_2^* \right\} \tag{23}$$

---

[*] Very little is known at present about the characteristics of waves of this type that are generated in hypervelocity impact. Hydrodynamic analyses[1, 4, 5] do not admit such waves, and they have apparently not been observed as yet in solutions which include material strength.[27]

where

$$\bar{Q}_o = \int_0^\infty \frac{N_1 e^{-\alpha z}}{N_1 - N_2} \, J_o(r\xi) \, J_1(a\xi) \, d\xi \tag{24}$$

$$\bar{Q}_1 = -\int_0^\infty \frac{N_1(N_1 + N_2)}{(N_1 - N_2)^2} \, e^{-\alpha(2h - z)} \, J_o(r\xi) \, J_1(a\xi) \, d\xi \tag{25}$$

$$\bar{Q}_2^* = \int_0^\infty \frac{2 N_1 N_2}{(N_1 - N_2)^2} \, e^{-h(\alpha + \beta) + \beta z} \, J_o(r\xi) \, J_1(a\xi) \, d\xi \tag{26}$$

In these expressions, J_o and J_1 denote Bessel functions of the first kind. The functions N_1, N_2, α, and β are given by

$$N_1 = \frac{2\mu c_1^2}{p^2} \left(\xi^2 + \frac{p^2}{2 c_2^2} \right)^2 \qquad\qquad N_2 = \frac{2\mu c_1^2}{p^2} \alpha\beta\xi^2 \tag{27}$$

$$\alpha = \sqrt{\xi^2 + p^2/c_1^2} \qquad\qquad \beta = \sqrt{\xi^2 + p^2/c_2^2} \tag{28}$$

In general, the inversion of these transforms is rather complicated, but can be effected by use of Cagniard's method.[28] The process is relatively simpler when applied to conditions along the axis of symmetry, particularly at the wavefronts. The remainder of this section is devoted to the extraction of these results.

Inversion of the Transforms

Thiruvenkatachar begins the inversion of these integrals by making the change of variable

$$\xi = \frac{p}{c_1} \eta \tag{29}$$

which leads to

$$\bar{Q}_0 = \frac{p}{c_1} \int_0^\infty \frac{A}{A-B} \exp\left[-\frac{pz}{c_1}\sqrt{1+\eta^2}\right] J_0\left(\frac{rp\eta}{c_1}\right) J_1\left(\frac{ap\eta}{c_1}\right) d\eta \tag{30}$$

$$\bar{Q}_1 = -\frac{p}{c_1} \int_0^\infty \frac{A(A+B)}{(A-B)^2} \exp\left[-\frac{p(2h-z)}{c_1}\sqrt{1+\eta^2}\right] J_0\left(\frac{rp\eta}{c_1}\right) J_1\left(\frac{ap\eta}{c_1}\right) d\eta \tag{31}$$

$$\bar{Q}_2^* = \frac{p}{c_1} \int_0^\infty \frac{2AB}{(A-B)^2} \exp\left[-\frac{p}{c_2}\left\{h\left(g\sqrt{1+\eta^2}+\sqrt{1+g^2\eta^2}\right) - z\sqrt{1+g^2\eta^2}\right\}\right] \times$$

$$\times \; J_0\left(\frac{rp\eta}{c_1}\right) J_1\left(\frac{ap\eta}{c_1}\right) d\eta \tag{32}$$

where

$$g = \frac{c_2}{c_1} = \frac{1}{\tilde{g}} \tag{33}$$

$$A = \left(1+2g^2\eta^2\right)^2 \qquad B = 4g^3\eta^2\sqrt{1+\eta^2}\sqrt{1+g^2\eta^2} \tag{34}$$

The next step is to use an integral representation for the Bessel-function product

$$J_0\left(\frac{pr\eta}{c_1}\right) J_1\left(\frac{pa\eta}{c_1}\right) = \frac{1}{\pi}\int_0^\pi J_1\left(\frac{p\eta R}{c_1}\right)\cos\chi \, d\phi \tag{35}$$

where R, χ, and ϕ are defined by
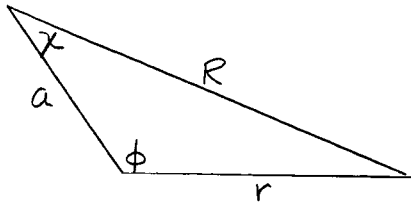
$$R^2 = a^2 + r^2 - 2ar\cos\phi$$

$$R\sin\chi = r\sin\phi \tag{36}$$

$$R\cos\chi = a - r\cos\phi$$

Note that χ depends on a, r, and ϕ, but not on η. If the remaining Bessel function is also replaced, by the integral representation

$$J_1\left(\frac{p\eta R}{c_1}\right) = \frac{p\eta R}{\pi c_1}\,\mathrm{Re}\int_0^\pi \exp\left[-i\,\frac{p\eta R}{c_1}\cos\psi\right]\sin^2\psi\,d\psi \tag{37}$$

and if the order of integration is changed, the result is

$$\bar{Q}_0 = \frac{p^2}{\pi^2 c_1^2}\,\mathrm{Re}\int_0^\pi (a - r\cos\phi)\int_0^\pi \sin^2\psi\ \times$$

$$\tag{38}$$

$$\times \int_0^\infty \frac{\eta A}{A - B}\exp\left[-\frac{p}{c_1}\left(z\sqrt{1+\eta^2} + i\eta R\cos\psi\right)\right]d\eta\,d\psi\,d\phi$$

$$\bar{Q}_1 = \frac{-p^2}{\pi^2 c_1^2}\,\mathrm{Re}\int_0^\pi (a - r\cos\phi)\int_0^\pi \sin^2\psi\ \times$$

$$\tag{39}$$

$$\times \int_0^\infty \frac{\eta A(A+B)}{(A-B)^2}\exp\left[-\frac{p}{c_1}\left([2h-z]\sqrt{1+\eta^2} + i\eta R\cos\psi\right)\right]d\eta\,d\psi\,d\phi$$

$$\bar{Q}_2^{\,*} = \frac{p^2}{\pi^2 c_1^2}\,\mathrm{Re}\int_0^\pi (a - r\cos\phi)\int_0^\pi \sin^2\psi\ \times$$

$$\tag{40}$$

$$\times \int_0^\infty \frac{2\eta AB}{(A-B)^2}\exp\left[-\frac{p}{c_2}\left\{h\left(q\sqrt{1+\eta^2} + \sqrt{1+q^2\eta^2}\right) - z\sqrt{1+q^2\eta^2} + iq\eta R\cos\psi\right\}\right]d\eta\,d\psi\,d\phi$$

Cagniard's technique is now applied to these, by making the changes of variable, in (38), (39), and (40), respectively

$$c_1 t = z\sqrt{1+\eta^2} + i\eta R\cos\psi \qquad (41)$$

$$c_1 t = (2h-z)\sqrt{1+\eta^2} + i\eta R\cos\psi \qquad (42)$$

$$c_2 t = h\left(q\sqrt{1+\eta^2} + \sqrt{1+q^2\eta^2}\right) - z\sqrt{1+q^2\eta^2} + iq\eta R\cos\psi \qquad (43)$$

As η varies from zero to infinity, t traces out a path in the complex plane:
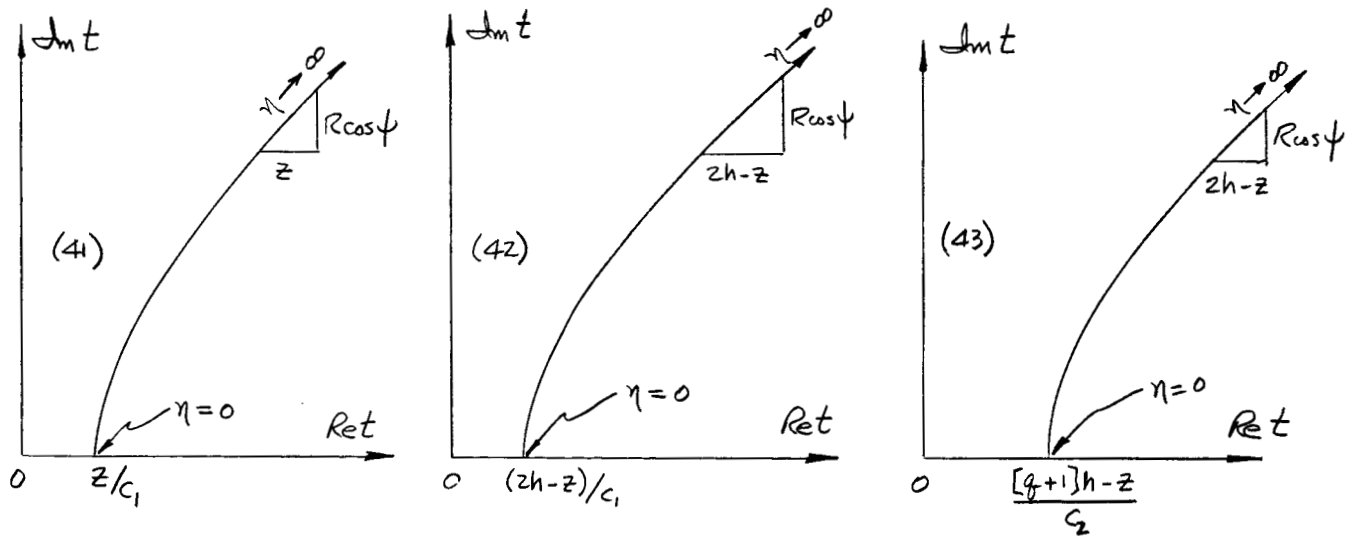
The path of integration can be deformed,[28] so that it lies along the real axis in the t-plane, and the result is

$$\bar{Q}_0 = \frac{p^2}{\pi^2 c_1^2}\, Re\int_{z/c_1}^{\infty} e^{-pt}\left[\int_0^{\pi}(a-r\cos\phi)\int_0^{\pi}\sin^2\psi\, F_1\left(\eta(t)\right)\frac{d\eta}{dt}\, d\psi\, d\phi\right] dt \qquad (44)$$

AI-1821-A-3

$$\bar{Q}_1 = \frac{-p^2}{\pi^2 c_1^2} \, Re \int_{\frac{2h-z}{c_1}}^{\infty} e^{-pt} \left[\int_0^{\pi} (a - r\cos\phi) \int_0^{\pi} \sin^2\psi \; F_2\left(\eta(t)\right) \frac{d\eta}{dt} \, d\psi \, d\phi \right] dt \quad (45)$$

$$\bar{Q}_2^* = \frac{p^2}{\pi^2 c_1^2} \, Re \int_{\frac{(q+1)h-z}{c_2}}^{\infty} e^{-pt} \left[\int_0^{\pi} (a - r\cos\phi) \int_0^{\pi} \sin^2\psi \; F_3\left(\eta(t)\right) \frac{d\eta}{dt} \, d\psi \, d\phi \right] dt \quad (46)$$

where

$$F_1(\eta) = \frac{\eta A}{A-B} \quad ; \quad F_2(\eta) = \frac{\eta A(A+B)}{(A-B)^2} \quad ; \quad F_3(\eta) = \frac{2\eta AB}{(A-B)^2} \quad (47)$$

and where the (complex) variable η is defined as an implicit function of the (real) variable t by Eqs. (41) - (43), respectively. Equations (44) - (46) can now be inverted by inspection. If r is set equal to zero, the contributions of the three waves to the stress along the axis of symmetry are found to be

$$\left.\bar{\sigma}_z\right)_P = \frac{Pa^2}{\pi c_1^2} \, p\,\bar{g}_1(p) \; ; \; \left.\bar{\sigma}_z\right)_{PP} = -\frac{Pa^2}{\pi c_1^2} \, p\,\bar{g}_2(p) \; ; \; \left.\bar{\sigma}_z\right)_{PS} = \frac{Pa^2}{\pi c_1^2} \, p\,\bar{g}_3(p) \quad (48)$$

where

$$g_1(t) = 1\left(t - \frac{z}{c_1}\right) \, Re \int_0^{\pi} \sin^2\psi \; F_1 \, \frac{d\eta}{dt} \, d\psi \quad (49)$$

$$q_2(t) = 1\left(t - \frac{2h-z}{c_1}\right) \text{Re} \int_0^\pi \sin^2\psi \; F_2 \frac{d\eta}{dt} \; d\psi \tag{50}$$

$$q_3(t) = 1\left(t - \frac{(q+1)h-z}{c_2}\right) \text{Re} \int_0^\pi \sin^2\psi \; F_3 \frac{d\eta}{dt} \; d\psi \tag{51}$$

and where R is to be replaced by a in Eqs. (41) - (43). If the limit $a \rightarrow 0$, $P \rightarrow \infty$ is now taken, with $Pa^2 = F/\pi$, then η no longer depends on ψ; the integrals in (49) - (51) can be worked out, and the result is

$$\frac{2\pi c_1^2}{F} \left.\sigma_z\right)_P = \frac{d}{dt}\left\{ 1\left(t - z/c_1\right) F_1 \frac{d\eta}{dt} \right\} \tag{52}$$

$$\frac{2\pi c_1^2}{F} \left.\sigma_z\right)_{PP} = \frac{d}{dt}\left\{ 1\left(t - \frac{2h-z}{c_1}\right) F_2 \frac{d\eta}{dt} \right\} \tag{53}$$

$$\frac{2\pi c_1^2}{F} \left.\sigma_z\right)_{PS} = \frac{d}{dt}\left\{ 1\left(t - \frac{(q+1)h-z}{c_2}\right) F_3 \frac{d\eta}{dt} \right\} \tag{54}$$

In these last three equations, η is defined as an implicit function of t by Eqs. (41) - (43), with $R = 0$.

Stress Discontinuities at the Wavefronts

Along each wavefront, γ is zero. The values of the stresses $\sigma_z)_P$, $\sigma_z)_{PP}$, $\sigma_z)_{PS}$ at the wavefront can be determined relatively easily, and are found to be

$$\sigma_z\Big)_P = \frac{F}{2\pi z^2}\left(1 + 8q^3\right) \quad , \quad \text{for} \quad z = c_1 t \tag{55}$$

$$\sigma_z\Big)_{PP} = \frac{-F}{2\pi(2h-z)^2}\left(1 + 24q^3\right) , \quad \text{for} \quad z = 2h - c_1 t \tag{56}$$

$$\sigma_z\Big)_{PS} = \frac{8Fq^3}{\pi\left[h - (h-z)q\right]^2} , \quad \text{for} \quad z = (q+1)h - c_2 t \tag{57}$$

In crossing any given wave, the contributions from the other two waves are continuous; thus Eqs. (55) - (57) also give the stress discontinuities that occur across the various waves.

All of the foregoing formulas agree with Davids' results.[26] Equations (55) - (57), for example, can be used to recover the stress discontinuities shown in Fig. 8 of Ref. 26, and can also be derived from the general formulas given there. Other checks can also be made; for example, Eqs. (55) - (57) add up to zero at the free surface $z = h$.

The most striking feature of the expressions for the stress discontinuities lies in the fact that they differ considerably from those describing spherically symmetric waves. In particular, the simple source-plus-image approximation would say that the formula for the jump in stress across the reflected dilatational wave ought to be derivable from the incident stress

formula $\left[\text{Eq. (55)}\right]$ by changing the sign, and replacing z by $2h-z$.
But such is not the case. A compression wave of unit amplitude is re-
flected as a tensile wave of amplitude $\left(1+24q^3\right)\big/\left(1+8q^3\right)$, a number
which is typically on the order of two. The reflected shear wave then im-
parts the amount of compression needed to preserve the zero stress condi-
tion at the free surface. Moreover, the contribution from the reflected
shear wave is nonzero even at $z = h$, in further contrast to the spheri-
cally symmetric case
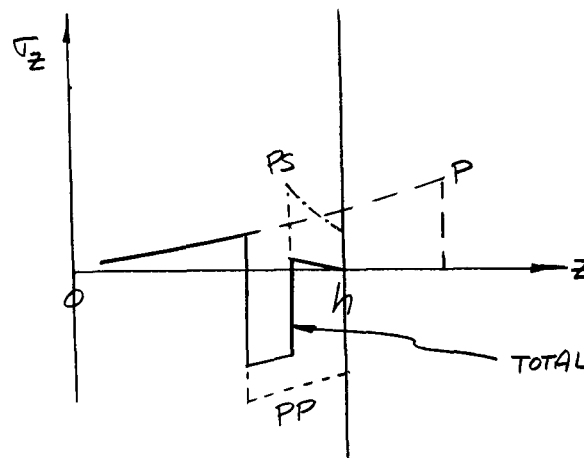
It is clear that such an amplification of the tensile stresses generated
upon reflection has an important bearing on the spall fracture problem. To
fully assess its importance, however, two factors must be examined. The
first is to determine how the amplification factor for reflected waves de-
pends on the degree of departure from spherical symmetry. Unfortunately,
there is no information available at present that might be used to infer this
dependence. The second item requiring attention is to determine how far
the incident stress distributions encountered in hypervelocity impact depart
from spherical symmetry. At present, the only pertinent information avail-
able consists of the pressure distributions found in the numerical solutions.

V. SPHERICAL POINT-SOURCE SOLUTION

The discussion of the two previous sections indicates that a definitive solution for reflected stress profiles cannot be given until the effect of off-axis variations in the incident stresses have been examined more fully. In spite of this reservation, it is nevertheless instructive to pursue the solution of the spherically symmetric case further. This section presents such a study, using for the excitation a point source instead of a cavity of finite radius. The purpose of this section is twofold: first, to show explicitly how the classical results of Cagniard,[28] long known in the field of seismology, can be applied to the present problem; and second, to arrive at some very general conclusions about the shape of the reflected stress profile and the influence of the incident profile by writing the solution in terms of a Duhamel integral.

Basic Relations

The coordinate system is the same as that used earlier, except that some new notation is introduced[*]

---
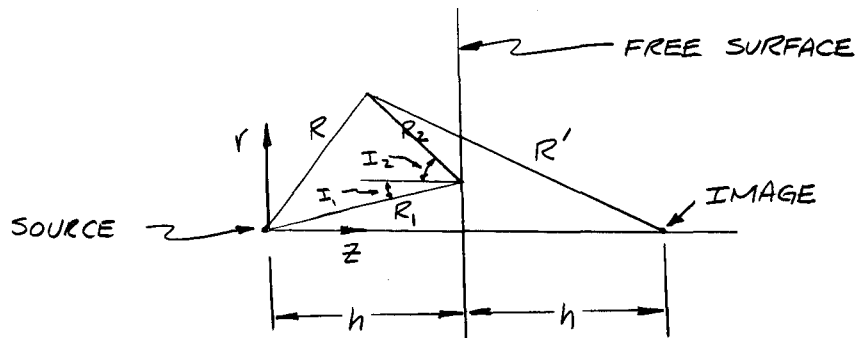
[*] The z-coordinate used here would be $h-z$ in Cagniard's[28] notation. Thus, the r-displacements and the derivatives $\partial/\partial z$ used here differ by a sign from those of Cagniard. The stress σ_z , which involves only $\partial r/\partial z$, can be taken directly from Cagniard's results by simply replacing z by $h-z$.

AI-1821-A-3

R and R' denote distance from the source and image, respectively, while R_1 and R_2 describe the minimum-time path for a wave that travels from the source to the free surface at the dilatational-wave speed, and thence to the field point r, z at the shear-wave speed. The angles I_1 and I_2 and the distances R_1 and R_2 are determined from the relations (for given r and z)

$$\frac{\sin I_1}{\sin I_2} = \frac{c_1}{c_2} = q \qquad r = R_1 \sin I_1 + R_2 \sin I_2$$

$$\tag{58}$$

$$h = R_1 \cos I_1 \qquad h - z = R_2 \cos I_2$$

In terms of the displacement potentials defined in Eq. (7),[*] the stress component σ_z along the axis of symmetry $r = 0$ is

$$\left. \sigma_z \right)_{r=0} = 2\lambda \left. \frac{\partial^2 \phi}{\partial r^2} \right)_{r=0} + (\lambda + 2\mu) \left. \frac{\partial^2 \phi}{\partial z^2} \right)_{r=0} + 4\mu \left. \frac{\partial^2 \psi}{\partial z \partial r} \right)_{r=0} \tag{59}$$

Method of Solution

Cagniard[28] writes the general solution in terms of two influence functions A and B :

$$\phi = \int_0^t F'(t-\tau) A(\tau ; r, z) \, d\tau \tag{60}$$

$$\psi = \int_0^t F'(t-\tau) B(\tau ; r, z) \, d\tau \tag{61}$$

---

[*] Cagniard[28] uses ψ and U for what are called ϕ and ψ , respectively, in this report.

where $F(t)$, the displacement potential at the source, is considered for present purposes to be given in terms of the incident stress distribution by Eq. (2).

The values of A and B change discontinuously at various instants, signalling the arrival of various waves. Thus in taking the derivatives called for in Eq. (59) under the integral signs in Eqs. (60) and (61), there will be contributions from the r - and z -dependence of the integration limits. For the moment, these contributions will be ignored; they will be added later. Carrying the derivatives under the integral sign gives

$$\frac{\sigma_z)_{r\to 0}}{\lambda+2\mu} = \int_0^t F'(t-\tau)\left\{\frac{2\lambda}{\lambda+2\mu}\frac{\partial^2 A}{\partial r^2} + \frac{\partial^2 A}{\partial z^2} + \frac{4\mu}{\lambda+2\mu}\frac{\partial^2 B}{\partial r \partial z}\right\}_{r=0} d\tau \qquad (62)$$

By use of the Laplace transform, Cagniard shows that[*]

$$A(\tau) = \begin{cases} 0, & \tau < RS \\ \frac{1}{R} - \frac{1}{R'} + A_3(\tau), & \tau > RS \end{cases} \qquad (63)$$

where the transform of A_3 is

$$\int_0^\infty e^{-p\tau} A_3(\tau) d\tau = -2\int_0^\infty \frac{bu^3 J_0(pur)}{D(u)} e^{-pa(2h-z)} du \qquad (64)$$

and where

$$a = \sqrt{u^2 + S^2} \quad , \quad b = \sqrt{u^2 + s^2}$$
$$D(u) = \left(u^2 + s^2/2\right)^2 - abu^2 \qquad (65)$$

The three terms in Eq. (63) correspond to a source, an image of opposite sign, and a third term caused by the surface shear stresses.

The transform of $B(\tau)$ is

$$\int_0^\infty e^{-p\tau} B(\tau)\, d\tau =$$

$$= \frac{2}{p} \int_0^\infty \frac{u(u^2 + s^2/2)}{D(u)} \frac{d}{dr}\left[J_0(pur) \right] e^{-p\left[ah + b(h-z) \right]}\, du \tag{66}$$

Inversion of the Transforms for $r = 0$

Most of the emphasis in Cagniard's treatment is on the case where $r/h \gg 1$, the case of greatest interest to seismologists, and the inversion of the transforms is a fairly complicated problem. The case considered here, $r = 0$, is the opposite extreme, and Cagniard's procedure for inverting the Laplace transforms can be applied very simply. Differentiating Eq. (64) twice with respect to r gives

$$\int_0^\infty e^{-p\tau} \frac{\partial^2 A_3}{\partial r^2}\, d\tau = 2 p^2 \int_0^\infty \frac{bu^5}{D(u)}\left[J_0(pur) - \frac{J_1(pur)}{pur} \right] e^{-pa(2h-z)}\, du \tag{67}$$

As $r \rightarrow 0$

$$\frac{1}{p^2}\int_0^\infty e^{-p\tau}\left(\frac{\partial^2 A_3}{\partial r^2} \right)_{r=0} d\tau = \int_0^\infty \frac{bu^5}{D(u)} e^{-pa(2h-z)}\, du \tag{68}$$

and with the new variable

$$\tau = a(2h - z) = \sqrt{u^2 + s^2}\,(2h - z) \tag{69}$$

Eq. (68) becomes

35   AI-1821-A-3

$$\int_0^\infty e^{-p\tau}\left[\int_0^\tau \int_0^\tau \left(\frac{\partial^2 A_3}{\partial r^2}\right)_{r=0} d\tau\, d\tau\right] d\tau = \int_{S(2h-z)}^\infty \frac{bu^4}{D} e^{-p\tau} \frac{\tau\, d\tau}{(2h-z)^2} \tag{70}$$

All functions in the integrand on the right are considered to be functions of τ ; for example, $D = D\left[u(\tau)\right]$. The inversion can now be accomplished by inspection, giving

$$\int_0^\tau \left(\frac{\partial^2 A_3}{\partial r^2}\right)_{r=0} d\tau \quad = \quad 0 \quad , \quad \tau < S(2h-z)$$

$$\tag{71}$$

$$= \frac{\partial}{\partial \tau}\left\{\frac{bu^4 \tau}{(2h-z)^2 D}\right\} \quad , \quad \tau > S(2h-z)$$

The reason for evaluating this first integral, rather than the function itself, is to facilitate a later integration by parts. Exactly the same series of steps can be used to show that

$$\int_0^\tau \left(\frac{\partial^2 A_3}{\partial z^2}\right)_{r=0} d\tau \quad = 0 \quad , \quad \tau < S(2h-z)$$

$$\tag{72}$$

$$= \frac{\partial}{\partial \tau}\left\{-2\frac{bu^2 a^2 \tau}{(2h-z)^2 D}\right\} \quad , \quad \tau > S(2h-z)$$

where, as in (71), $u(\tau)$ is defined by Eq. (69).

Differentiating Eq. (66) with respect to r and z , and setting $r = 0$ gives

$$\frac{1}{p^2}\int_0^\infty e^{-p\tau}\left(\frac{\partial^2 B}{\partial r \partial z}\right)_{r=0} d\tau =$$

$$\tag{73}$$

$$= \int_0^\infty \frac{bu^3(u^2 + s^2/2)}{D(u)} e^{-p\left[ah + b(h-z)\right]} du$$

AI-1821-A-3

In this case, the appropriate change of variable is

$$\tau = ah + b(h-z) = \sqrt{u^2 + S^2}\, h + \sqrt{u^2 + s^2}\,(h-z) \qquad (74)$$

which after inversion leads to

$$\int_0^\tau \left(\frac{\partial^2 B}{\partial r \partial z}\right)_{r=0} d\tau = 0 \qquad , \quad \tau < Sh + s(h-z) \qquad (75)$$

$$= \frac{\partial}{\partial \tau}\left\{ \frac{bu^2(u^2 + s^2/2)}{D\left[h/a + (h-z)/b \right]} \right\} \quad , \quad \tau > Sh + s(h-z)$$

It is useful to put these results in dimensionless form, by introducing the notation

$$u = Sx \quad , \quad a = S\alpha = S\sqrt{x^2 + 1} \quad , \quad b = S\beta = S\sqrt{x^2 + q^2}$$

$$D = S^4 \mathcal{D} = S^4\left\{ \left(x^2 + q^2/2\right)^2 - \alpha\beta x^2 \right\}$$

$$\frac{dD}{du} = S^3 \mathcal{D}' = S^3\left\{ 4x\left(x^2 + q^2/2\right) - \frac{\beta x^3}{\alpha} - \frac{\alpha x^3}{\beta} - 2\alpha\beta x \right\} \qquad (76)$$

$$V_1 = c_1 h^2 \frac{2\lambda}{\lambda + 2\mu} \int_0^\tau \left(\frac{\partial^2 A_3}{\partial r^2}\right)_{r=0} d\tau$$

$$V_2 = c_1 h^2 \int_0^\tau \left(\frac{\partial^2 A_3}{\partial z^2}\right)_{r=0} d\tau$$

$$V_3 = c_1 h^2 \frac{4\mu}{\lambda + 2\mu} \int_0^\tau \left(\frac{\partial^2 B}{\partial r \partial z}\right)_{r=0} d\tau$$

where $(\ )'$ means d/dx .

When the differentiations with respect to τ indicated in Eqs. (71), (72), and (75) are carried out, and the results expressed according to the notation in Eq. (76), the results are:

AI-1821-A-3

$$\left(V_1 + V_2\right)\left(2 - \frac{z}{h}\right)^2 = \frac{2\nu}{1-\nu}\left\{ \zeta^2 \frac{x^2}{\mathcal{D}}\left[\frac{x^2}{\beta} + 4\beta - \frac{\beta x \mathcal{D}'}{\mathcal{D}}\right] + \frac{\beta x^4}{\mathcal{D}} \right\}$$

(77)

$$- 2\left\{ \zeta^2 \frac{\alpha}{\mathcal{D}}\left[\frac{x^2\alpha}{\beta} + 2\alpha\beta + \frac{2\beta x^2}{\alpha} - \frac{\alpha\beta x \mathcal{D}'}{\mathcal{D}}\right] + \frac{\alpha^2\beta x^2}{\mathcal{D}} \right\}$$

$$V_3 = \frac{2(1-2\nu)}{1-\nu}\frac{\alpha\beta}{\left[\beta + (1-z/h)\alpha\right]^2}\left\{ \frac{\beta}{\mathcal{D}}\sqrt{\mathcal{D} + \alpha\beta x^2}\left[2\alpha\beta \right.\right.$$

(78)

$$\left. + \frac{x^2\beta}{\alpha} + \frac{2x^2\alpha}{\beta} - \frac{x\alpha\beta\mathcal{D}'}{\mathcal{D}} - x^2\frac{\alpha + (1-z/h)\beta}{\beta + (1-z/h)\alpha}\right] + \frac{2x^2\alpha\beta^2}{\mathcal{D}} \right\}$$

In Eq. (77), the parameter ζ is defined as

$$\zeta = \frac{c_1 \tau / h}{2 - z/h}$$

(79)

and the quantities x, $\mathcal{D}$, α, β, and $\mathcal{D}'$ are all functions of ζ, given by Eq. (69), which becomes

$$x = \sqrt{\zeta^2 - 1}$$

(80)

In Eq. (78), the functions α, β, $\mathcal{D}$, and $\mathcal{D}'$ are the same functions of x as before (defined in Eq. (76)), but the dependence of x on τ and z is different. It is given by Eq. (74), which becomes:

$$\frac{c_1 \tau}{h} = \sqrt{x^2 + 1} + \left(1 - \frac{z}{h}\right)\sqrt{x^2 + q^2}$$

(81)

The inversion of this leads to a quadratic in x^2, the correct solution of which uses the minus sign:

AI-1821-A-3

$$X = \left\{ \frac{-b_3 - \sqrt{b_3^2 - 4a_3 C_3}}{2a_3} \right\}^{1/2} \tag{82}$$

where

$$a_3 = \left[\left(1 - \frac{z}{h} \right)^2 - 1 \right]^2$$

$$b_3 = 2 \left[\left(1 - \frac{z}{h} \right)^2 - 1 \right] \left[g^2 \left(1 - \frac{z}{h} \right)^2 - 1 - \left(\frac{c_1 \tau}{h} \right)^2 \right] - 4 \left(\frac{c_1 \tau}{h} \right)^2 \tag{83}$$

$$C_3 = \left[g^2 \left(1 - \frac{z}{h} \right)^2 - 1 - \left(\frac{c_1 \tau}{h} \right)^2 \right]^2 - 4 \left(\frac{c_1 \tau}{h} \right)^2$$

The functions $(V_1 + V_2) \left(2 - \frac{z}{h} \right)^2$, and V_3 are shown in Figs. 4 and 5 for $\nu = 1/4$. V_1 and V_2 are zero for $\zeta < 1$, while V_3 is zero for $\frac{c_1 \tau}{h} < 1 + g \left(1 - \frac{z}{h} \right)$. It should be noted that the sum $V_1 + V_2 + V_3$ vanishes at the free surface $\frac{z}{h} = 1$.

Terms Arising from the Limits

When taking derivatives under the integral sign in finding the expression for σ_z , terms arising from the r- and z-dependence of the integration limits were omitted. These terms must now be added. During the time interval between the arrival of the incident dilatational wave and that of the reflected dilatational wave, the potentials are simply

$$A = \frac{1}{R} \quad , \quad B = 0 \tag{84}$$

and the corresponding stress along the axis is that given earlier in Eq. (4)

$$\frac{\sigma_z}{\lambda + 2\mu} = \frac{S^2 F''(-)}{z} + \frac{2(1-2\nu)}{1-\nu} \left\{ \frac{SF'(-)}{z^2} + \frac{F(-)}{z^3} \right\} \tag{85}$$

where the argument $t - Sz$ is denoted by $(-)$. After arrival of the reflected dilatational wave, but before the reflected shear wave, the potentials are $\psi = 0$, and

$$\phi = \frac{1}{R} \int_{RS}^{R'S} F'(t-\tau) d\tau + \left(\frac{1}{R} - \frac{1}{R'}\right) \int_{R'S}^{t} F'(t-\tau) d\tau + \int_{R'S}^{t} F'(t-\tau) A_3 d\tau$$

(86)

$$= \frac{F(t-SR)}{R} - \frac{F(t-SR')}{R'} + \int_{SR'}^{t} F'(t-\tau) A_3(\tau) d\tau$$

In arriving at the first two terms of this expression, $F(o)$ is taken to be zero (as is $F'(o)$ below) in accordance with Cagniard's procedure for evaluating the discontinuities in the solution. Differentiating Eq. (86) twice with respect to r leads to a very lengthy expression involving, among other things, $\partial R / \partial r$, $\partial R' / \partial r$, $\partial^2 R / \partial r^2$, and $\partial^2 R' / \partial r^2$, where

$$R = \sqrt{r^2 + z^2} \quad , \quad R' = \sqrt{r^2 + (2h-z)^2}$$

(87)

When $r \to o$,

$$\frac{\partial R}{\partial r} = \frac{\partial R'}{\partial r} = 0 , \quad \frac{\partial^2 R}{\partial r^2} \longrightarrow \frac{1}{z} , \quad \frac{\partial^2 R'}{\partial r^2} \longrightarrow \frac{1}{2h-z}$$

(88)

Many of the terms in the lengthy expression for $\partial^2 \phi / \partial r^2$ vanish when $r = 0$, leaving:

$$\frac{\partial^2 \phi}{\partial r^2}\bigg)_{r \to o} = \frac{-1}{z} \left\{ \frac{SF'(-)}{z} + \frac{F(-)}{z^2} \right\} + \frac{1}{2h-z} \left\{ \frac{SF'(+)}{2h-z} + \frac{F(+)}{(2h-z)^2} \right.$$

(89)

$$\left. - SF'(+) A_3 \left(S(2h-z); 0, z \right) \right\} + \int_{S(2h-z)}^{t} F'(t-\tau) \left(\frac{\partial^2 A_3}{\partial r^2}\right)_{r=0} d\tau$$

AI-1821-A-3

where the argument $t - S(2h-z)$ is denoted by $(+)$. The derivative $\partial^2\phi/\partial z^2\big)_{r\to 0}$ can be worked out in similar fashion, using the fact that, as $r \to 0$,

$$\frac{\partial R}{\partial z} \to +1, \quad \frac{\partial R'}{\partial z} \to -1, \quad \frac{\partial^2 R}{\partial z^2} \to 0, \quad \frac{\partial^2 R'}{\partial z^2} \to 0 \tag{90}$$

The result is

$$\frac{\partial^2\phi}{\partial z^2}\bigg)_{r\to 0} = S^2 \frac{F''(-)}{z} + \frac{2SF'(-)}{z^2} + \frac{2F(-)}{z^3} - S^2 \frac{F''(+)}{2h-z} - \frac{2SF'(+)}{(2h-z)^2} - \frac{2F(+)}{(2h-z)^3} \tag{91}$$

$$+ F''(+) A_3\left(S(2h-z); 0, z\right) - S^2 F'(+) \frac{\partial A_3}{\partial \tau}\left(S(2h-z); 0, z\right)$$

$$-2SF'(+) \frac{\partial A_3}{\partial z}\left(S(2h-z); 0, z\right) + \int_{S(2h-z)}^{t} F'(t-\tau) \left(\frac{\partial^2 A_3}{\partial z^2}\right)_{r=0} d\tau$$

When the reflected shear wave passes, the terms derived from ϕ do not change, but a new contribution comes from ψ

$$\psi = \int_{SR_1 + sR_2}^{t} F'(t-\tau) B(\tau; r, z) d\tau \tag{92}$$

When the mixed derivative of this quantity with respect to r and z is formed, and evaluated for $r = 0$, it becomes necessary to know certain derivatives of R_1 and R_2 . These are most easily worked out by using the approximate form of Eqs. (58) valid for $r \to 0$
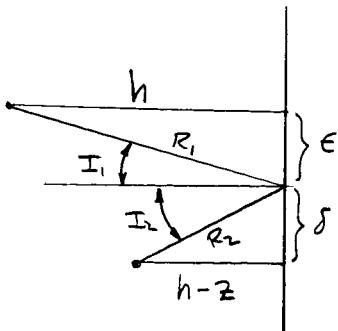
$$r = \epsilon + \delta$$

$$R_1 = h + O(r^2) \tag{93}$$

$$R_2 = h - z + O(r^2)$$

From Eq. (93) it follows that $\partial R_1/\partial r$, $\partial R_1/\partial z$, $\partial R_2/\partial r$,
$\partial^2 R_1/\partial r\partial z$, $\partial^2 R_2/\partial r\partial z$ are all zero at $r = 0$, while $\partial R_2/\partial z\big)_{r=0} = -1$.

The result is

$$\frac{\partial^2 \psi}{\partial r\partial z}\bigg)_{r=0} = - sF'\left(t- Sh - s(h-z)\right)\frac{\partial B}{\partial r}\left(Sh + s(h-z) ; 0, z\right)$$

$$+ \int_{Sh + s(h-z)}^{t} F'(t-\tau) \frac{\partial^2 B}{\partial r\partial z}\bigg)_{r=0} d\tau \tag{94}$$

If all the extra terms are now collected, and the convention used that F and all its derivatives are zero for negative argument, the complete expression for the stress becomes

$$\frac{\sigma_z)_{r=0}}{\lambda + 2\mu} = \frac{2\nu}{1-\nu}\left\{ - \frac{SF'(-)}{z^2} - \frac{F(-)}{z^3} + \frac{SF'(+)}{(2h-z)^2} + \frac{F(+)}{(2h-z)^3} \right\}$$

$$+ \frac{S^2 F''(-)}{z} + \frac{2SF'(-)}{z^2} + \frac{2F(-)}{z^3} - \frac{S^2 F''(+)}{2h-z} - \frac{2SF'(+)}{(2h-z)^2} - \frac{2F(+)}{(2h-z)^3}$$

$$\tag{95}$$

$$- \frac{2\nu}{1-\nu}\frac{SF'(+) A_3\left(S(2h-z); 0,z\right)}{2h-z} + S^2 F''(+) A_3\left(S(2h-z); 0, z\right) - S^2 F'(+)\frac{\partial A_3}{\partial z}\left(S(2h-z) ; 0, z\right)$$

$$-2SF'(+)\frac{\partial A_3}{\partial z}\left(S(2h-z); 0, z\right) - \frac{2(1-2\nu)}{1-\nu} sF'\left(t -Sh -s(h-z)\right)\frac{\partial B}{\partial r}\left(Sh + s(h-z) ; 0, z\right)$$

$$+ \int_{0}^{t} F'(t-\tau)\left\{ \frac{2\nu}{1-\nu}\frac{\partial^2 A_3}{\partial r^2} + \frac{\partial^2 A_3}{\partial z^2} + \frac{2(1-2\nu)}{1-\nu}\frac{\partial^2 B}{\partial r\partial z} \right\}_{r=0} d\tau$$

Further simplifications of this expression are now possible. The first two lines correspond to the solution that would be given by the source and its image. Some of the remaining terms are zero; by a straightforward application of Cagniard's method, it can be shown that

AI-1821-A-3

$$A_3\left(\tau; 0, z\right) = 0 \quad , \quad \tau < S\left(2h - z\right)$$

(96)

$$= \frac{-2bu^2\tau}{D(u)\left(2h-z\right)^2} \quad , \quad \tau > S\left(2h-z\right)$$

Thus $A_3\left(S(2h-z); 0, z\right) = 0$. By differentiating (96), it is found that

$$\left.\frac{\partial A_3}{\partial \tau}\right)_{\tau = S(2h-z)} = \frac{-16}{g^3 S\left(2h-z\right)^2}$$

(97)

and it can also be shown, either by differentiating (96) or by inverting $\partial A_3 / \partial z$, that

$$\left.\frac{\partial A_3}{\partial z}\right)_{\tau = S(2h-z)} = \frac{+16}{g^3 \left(2h-z\right)^2}$$

(98)

Finally, inverting $\partial B / \partial r$ reveals that

$$\left.\frac{\partial B}{\partial r}\right)_{\tau = Sh + s(h-z)} = \frac{-4}{g^2 h^2 \left(1 + \frac{h-z}{gh}\right)^2}$$

(99)

Thus Eq. (95) is reduced to

$$\frac{\sigma_z)_{r=0}}{\lambda + 2\mu} = \left.\frac{\sigma_z)_{r=0}}{\lambda + 2\mu}\right)_{SOURCE + IMAGE}$$

(100)

$$+ \int_0^t F'(t-\tau) \left\{\frac{2\nu}{1-\nu}\frac{\partial^2 A_3}{\partial r^2} + \frac{\partial^2 A_3}{\partial z^2} + \frac{2(1-2\nu)}{1-\nu}\frac{\partial^2 B}{\partial r \partial z}\right\}_{r=0} d\tau$$

$$- \frac{16 S F'(+)}{g^3 \left(2h-z\right)^2} + \frac{2(1-2\nu)}{1-\nu} s F'\left(t - Sh - s(h-z)\right)\frac{4}{g^2 h^2 \left(1 - {(h-z)}/{gh}\right)^2}$$

The last two terms can now be absorbed through an integration by parts.

Let

$$V_1 = \int_0^\tau \frac{2\nu}{1-\nu} \frac{\partial^2 A_3}{\partial r^2} \, d\tau \quad , \quad V_2 = \int_0^\tau \frac{\partial^2 A_3}{\partial z^2} \, d\tau \quad , \quad V_3 = \int_0^\tau \frac{2(1-2\nu)}{1-\nu} \frac{\partial^2 B}{\partial r \partial z} \, d\tau \tag{101}$$

Then

$$\int_0^t F'(t-\tau) \left\{ \frac{2\nu}{1-\nu} \frac{\partial^2 A_3}{\partial r^2} + \frac{\partial^2 A_3}{\partial z^2} + \frac{2(1-2\nu)}{1-\nu} \frac{\partial^2 B}{\partial r \partial z} \right\} d\tau =$$

$$= \left[F'(t-\tau)(V_1 + V_2) \right]_{S(2h-z)}^t + \left[F'(t-\tau) V_3 \right]_{Sh+s(h-z)}^t$$

$$+ \int_0^t F''(t-\tau)(V_1 + V_2 + V_3) \, d\tau \tag{102}$$

$$= -F'\!\left(t - S(2h-z)\right)\left[V_1 + V_2\right]_{\tau = S(2h-z)} - F'\!\left(t - Sh - s(h-z)\right)\left[V_3\right]_{\tau = Sh + s(h-z)}$$

$$+ \int_0^t F''(t-\tau)(V_1 + V_2 + V_3) \, d\tau$$

Since

$$\left(V_1 + V_2 \right)_{\tau = S(2h-z)} = \frac{(V_1 + V_2)_{J=1}}{c_1 h^2} = \frac{-16 S}{q^3 (2h-z)^2}$$

$$\left(V_3 \right)_{\tau = Sh + s(h-z)} = \frac{V_3)_{x=0}}{c_1 h^2} = \frac{16}{q^3 \left(1 + \frac{(h-z)}{qh} \right)^2} \tag{103}$$

The final expression for σ_z can be written in the form

$$\frac{\sigma_z)_{r=0}}{\lambda + 2\mu} = \frac{\sigma_z)_{r=0}}{\lambda + 2\mu} \bigg)_{\text{SOURCE + IMAGE}} + \int_0^t F''(t-\tau)(V_1 + V_2 + V_3) \, d\tau \tag{104}$$

44   AI-1821-A-3

The integral appearing here collects all of the corrections to the source-image solution that arise from the surface-distributed shear stress. It introduces no discontinuities, even at the reflected shear wave, and has the effect only of altering the profile.

Final Formula

It is useful to employ the dimensionless variables

$$\theta = \frac{c_1 \tau}{h} \ , \quad V = c_1 h^2 v \ , \quad F''(\tau) = c_1^2 h \ \mathcal{Y}''(\theta) \tag{105}$$

In terms of these, Eq. (104) becomes

$$\frac{\sigma_z)_{r=0}}{\lambda + 2\mu} = \left. \frac{\sigma_z)_{r=0}}{\lambda + 2\mu} \right)_{\text{SOURCE + IMAGE}} + \int_0^{c_1 t / h} \mathcal{Y}'' \left(\frac{c_1 t}{h} - \theta \right) V \left(\theta; \frac{z}{h}; v \right) d\theta \tag{106}$$

The function $\mathcal{Y}''$ appearing in this integrand is to be found from the incident stress profile, for example by the method described in Section II.

The variation of the influence function appearing in the integrand of Eq. (106) is shown in Fig. 6 for the case $z/h = 0.8$, $c_1 t / h = 1.5$, $v = 1/4$. For points as yet unaffected by the reflected shear wave, the effect of the integral is to contribute an additional tensile component. After passage of the shear wave, a compressive contribution is felt. Actually, the integral correction term will not be very great in cases where $\mathcal{Y}''$ falls sharply from its maximum, since the integrand rapidly becomes small under such circumstances.

General Conclusion

It must be emphasized that Eq. (106) is restricted to cases with spherically symmetric incident waves; for such cases, the integral in Eq. (106)

45   AI-1821-A-3

represents, in a general but concise way, the correction to the source-image system due to the surface-distributed shear stresses. Generally speaking, the correction term will have the effect of modifying the reflected-stress profile slightly, but will leave the maximum tensile stress unchanged, especially for profiles which decay rapidly.

VI. CONCLUDING REMARKS

It is well to reiterate in conclusion the approximation that forms the basis of this entire study, namely, the use of a linear elastic model. In applying the results above to the interpretation of spall-fracture experiments, serious reservations must be held concerning the effects of non-elastic response. These may affect the wave propagation itself. In addition, no attempt has been made to invoke a fracture criterion. Even if the linear elastic model is accepted, one must still decide whether or not the fracture stress is time-dependent. It is unfortunately the case that the results of spallation experiments are the product of an unknown mixture of wave-propagation effects and fracture-criterion effects. There would appear to be little hope of drawing firm conclusions about the relative importance of these two sources of uncertainty, except from experiments done in internally instrumented targets.

On the other hand, it is important, in constructing a rational theory for this problem, to be sure that all the implications of even the most primitive approximation are fully understood. One contribution of this research has been to reveal the significance of the simple source-image model. Results derived from such a model depart only slightly from the exact linear-elastic results for cases where the incident wave is spherically symmetric. For such cases, and for incident stress distributions which decrease rapidly behind the incident wave, the maximum tensile stress (on the axis of symmetry, at the wave front) can safely be calculated by the source-image model.

A more important result has been to call attention to the fact that the reflection laws inherent in the source-image model may be drastically

changed for cases where the incident stress distribution is not spherically symmetric. In such cases, compression waves of unit amplitude are reflected with more than unit amplitude from a free surface. Unfortunately, not enough is known about this solution at present to indicate the connection between the degree of amplification and the extent of departure from spherical symmetry.

One of the items necessary in elucidating these questions is a physical explanation of why an amplification occurs at all. It is also important that a study be made of incident stress distributions whose angular variations are intermediate between those of the spherically symmetric case and those generated by a point force. Finally, the extent of angular variations present in existing hydrodynamic and viscoplastic solutions should be examined.

Until a thorough investigation of these points is made, it must be recognized that there is no firm theoretical basis for many of the conventional rules of thumb often used in dealing with spall fracture -- for example the unit reflection coefficient, and the relation between the spall thickness and the wavelength of the incident disturbance.

AI-1821-A-3

REFERENCES

1. Rae, W. J., Nonsimilar Solutions for Impact-Generated Shock Propagation in Solids. CAL Report AI-1821-A-2, NASA CR 54251 (Jan. 1965).

2. Loeffler, I. J., Lieblein, S., and Clough, N., Meteoroid Protection for Space Radiators. Pages 551-579 of Power Systems for Space Flight, Ed. by M. A. Zipkin and R. N. Edwards. Volume 11 of Progress in Astronautics and Aeronautics, Academic Press, New York, 1963.

3. Anderson, D. C., Fisher, R. D., McDowell, E. L., and Weidermann, A. H., Close-In Effects from Nuclear Explosions. AFSWC TDR-63-53 (May 1963) AD 411 132.

4. Walsh, J. M., Johnson, W. E., Dienes, J. K., Tillotson, J. H., and Yates, D. R., Summary Report on the Theory of Hypervelocity Impact. General Atomic Division, General Dynamics Corp., Report GA-5119 (March 31, 1964).

5. Bjork, R. L., Effects of a Meteoroid Impact on Steel and Aluminum in Space. Tenth International Astronautical Congress Proceedings, Vol. II, Springer Verlag, pp. 505-514 (1960).

6. Bjork, R. L., Analysis of the Formation of Meteor Crater, Arizona: A Preliminary Report. J. Geophys. Res., Vol. 66, pp. 3379-3387 (1961).

7. Walsh, J. M., and Tillotson, J. H., Hydrodynamics of Hypervelocity Impact. General Atomic Division, General Dynamics Corp., Report GA-3827 (Jan. 22, 1963) AD 401 023. Also published in the Proceedings of the Sixth Symposium on Hypervelocity Impact, Vol. 2, Pt. I, pp. 59-104 (Aug. 1963).

8. Rae, W. J., and Kirchner, H. P., Final Report on a Study of Meteoroid Impact Phenomena. CAL Report RM-1655-M-4 (Feb. 1963) N63-16887.

9. Rae, W. J., and Kirchner, H. P., A Blast-Wave Theory of Crater Formation in Semi-Infinite Targets. Proceedings of the Sixth Symposium on Hypervelocity Impact, Vol. 2, Pt. 1, pp. 163-229 (Aug. 1963).

10. Davids, N., and Huang, Y. K., Shock Waves in Solid Craters. J. Aero/Space Sci., Vol. 29, pp. 550-557 (1962).

11. Calvit, H. H., and Davids, N., Spherical Shock Waves in Solids. Pennsylvania State University, Dept. of Engineering Mechanics, Technical Report No. 2 (July 9, 1963) AD 415617.

12. Cole, R. H., Underwater Explosions. Princeton University Press (1948).

13. Rice, M. H., McQueen, R. G., and Walsh, J. M., Compression of Solids by Strong Shock Waves. Solid State Physics, Advances in Research and Applications, Ed. by F. Seitz and D. Turnbull, Vol. 6, Academic Press, 1958.

14. Allen, W. A., and Goldsmith, W., Elastic Description of a High-Amplitude Spherical Pulse in Steel. J. Appl. Phys., Vol. 26, No. 1, pp. 69-74 (Jan. 1955).

15. Rinehart, J. S., and Pearson, J., Behavior of Metals under Impulsive Loads. American Society for Metals (1954).

16. Marcus, H., Comments on a paper by K. Broberg, p. 246, International Symposium on Stress Wave Propagation in Materials, Ed. by N. Davids, Interscience, New York, 1960.

17. Aliev, Kh. M., Reflection of Spherical Elastic Waves at the Boundary of a Half-Space. Zhurnal Prikladnoi Mekhaniki i Tekhnicheskoi Fiziki, No. 6, pp. 88-92 (Nov. - Dec. 1961) (In Russian).

18. Kinslow, R., Properties of Spherical Shock Waves Produced by Hypervelocity Impact. Proceedings of the Sixth Symposium on Hypervelocity Impact, Vol. 2, Pt. 1, pp. 273-320 (Aug. 1963).

19. Blake, F. G., Spherical Wave Propagation in Solid Media. J. Acoust. Soc. Am., Vol. 24, No. 2, pp. 211-215 (March 1952).

20. Karal, F. C., and Keller, J. B., Elastic Wave Propagation in Homogeneous and Inhomogeneous Media. J. Acoust. Soc. Am., Vol. 31, No. 6, pp. 694-705 (June 1959).

21. Bagdoev, A. G., Spatial Non-Stationary Motions of Solid Medium with Shock Waves. Publishing House of the Academy of Sciences of the Armenian SSR, Erevan, 1961. Translated as U. S. Atomic Energy Commission AEC TR-6400, Nov. 1962.

22. Huth, J. H., and Cole, J. D., Impulsive Loading on an Elastic Half-Space. J. Appl. Mech., Vol. 21, pp. 294-295 (Sept. 1954).

23. Thiruvenkatachar, V. R., Stress Waves Produced in a Semi-Infinite Elastic Solid by Impulse Applied over a Circular Area of the Plane Face. Proceedings of the First Congress on Theoretical and Applied Mechanics, Nov. 1 - 2, 1955. Published by the Indian Society of Theoretical and Applied Mechanics, Indian Institute of Technology, Kharagpur, India.

24. Thiruvenkatachar, V. R., Recent Research in Stress Waves in India. Pages 1-14 of the Proceedings of an International Symposium on Stress Wave Propagation in Materials, Ed. by N. Davids, Interscience Pub., New York, 1960.

25. Broberg, K. B., A Problem on Stress Waves in an Infinite Elastic Plate. Transactions of the Royal Institute of Technology, Stockholm, Sweden, No. 139 (1959).

26. Davids, N., Transient Analysis of Stress-Wave Penetration in Plates. J. Appl. Mech., Vol. 26, pp. 651-660 (Dec. 1959).

27. Riney, T. D., Theoretical Hypervelocity Impact Calculations using the Picwick Code. General Electric Co. Report R64SD13 (Feb. 1964).

28. Cagniard, L., Reflection and Refraction of Progressive Seismic Waves. Translated and revised by E. A. Flinn and C. H. Dix, McGraw-Hill, 1962.
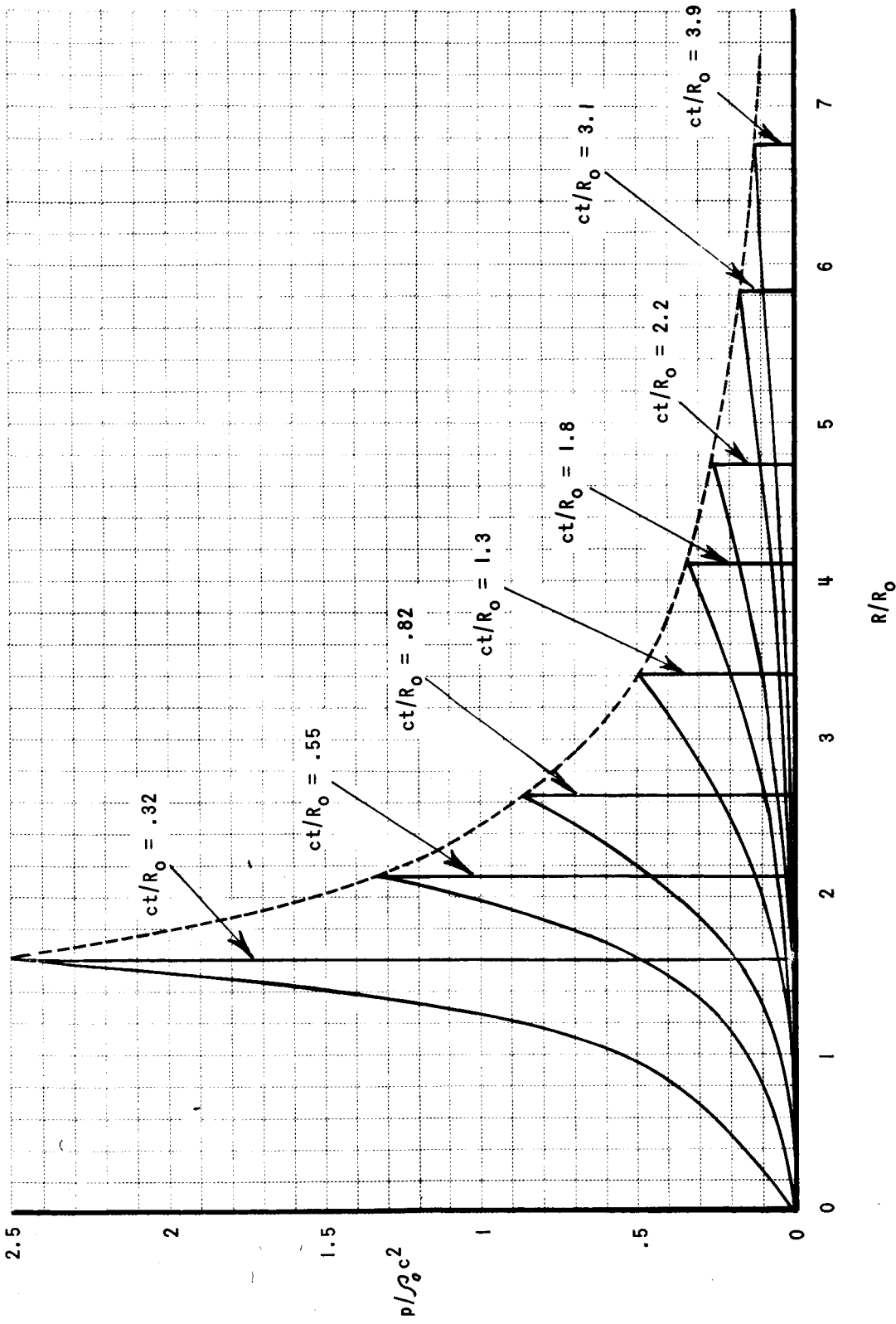
Figure I PRESSURE DISTRIBUTION ACCORDING TO QUASI-STEADY THEORY, S = 1.5

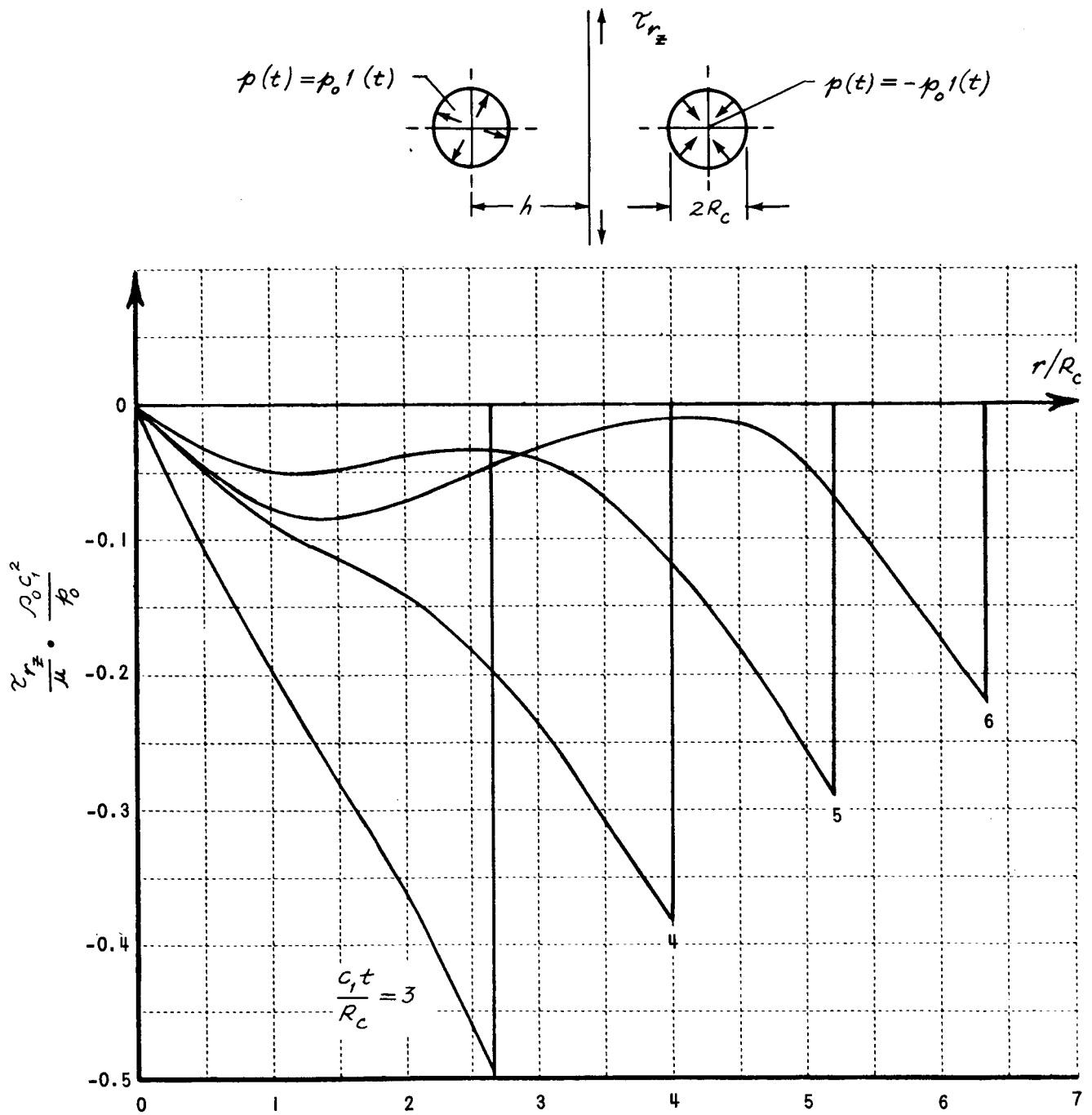$$R_o \equiv (E/2\pi \rho_o c^2)^{1/3}$$

AI-1821-A-3

Figure 2 SURFACE SHEAR STRESS PRODUCED BY SOURCE AND IMAGE CAVITIES

$$R_c/h = 1/3, \ \nu = 1/4$$
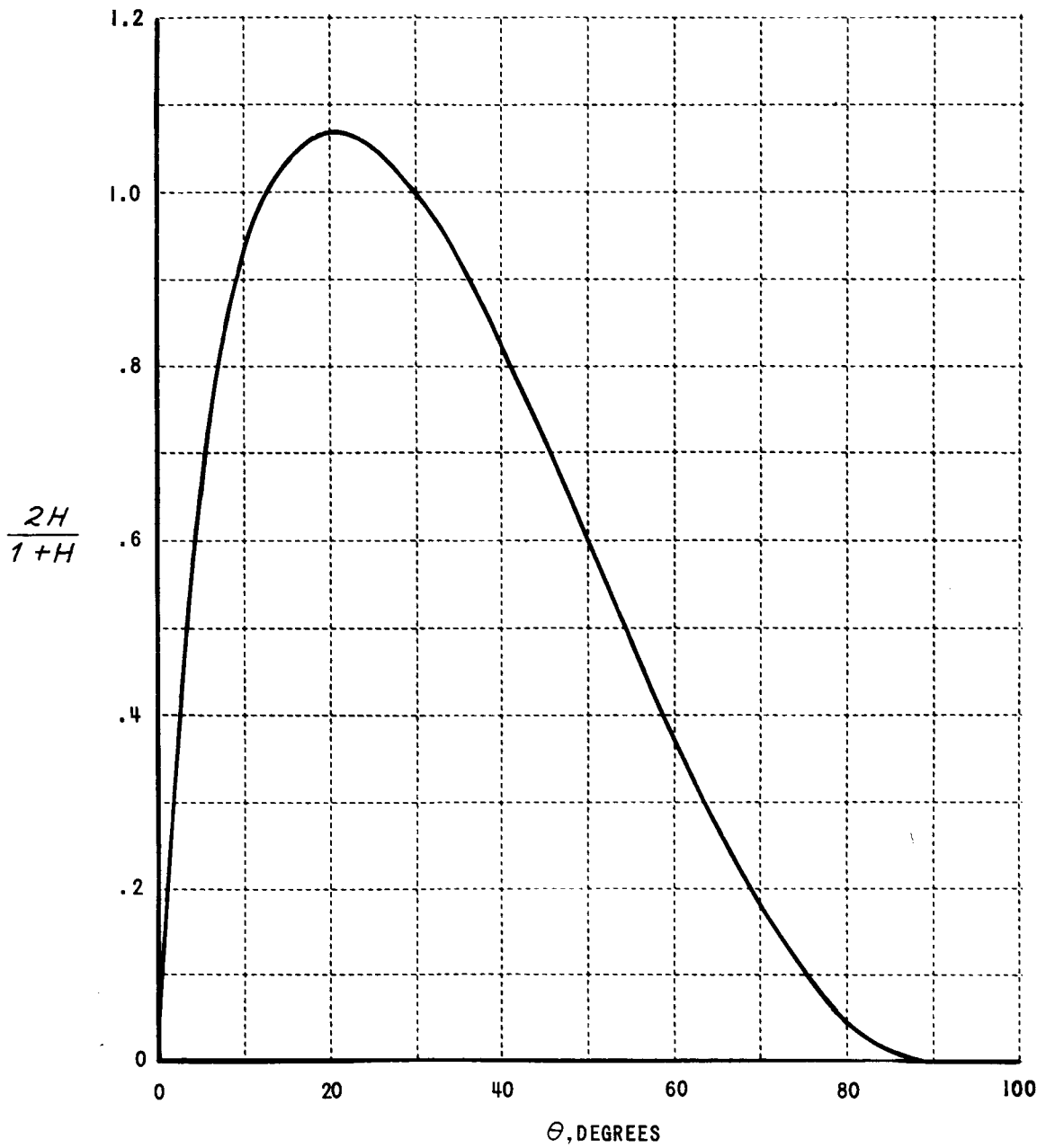
AI-1821-A-3

Figure 3   THE FUNCTION $H(\theta)$, FOR $\nu = 1/4$
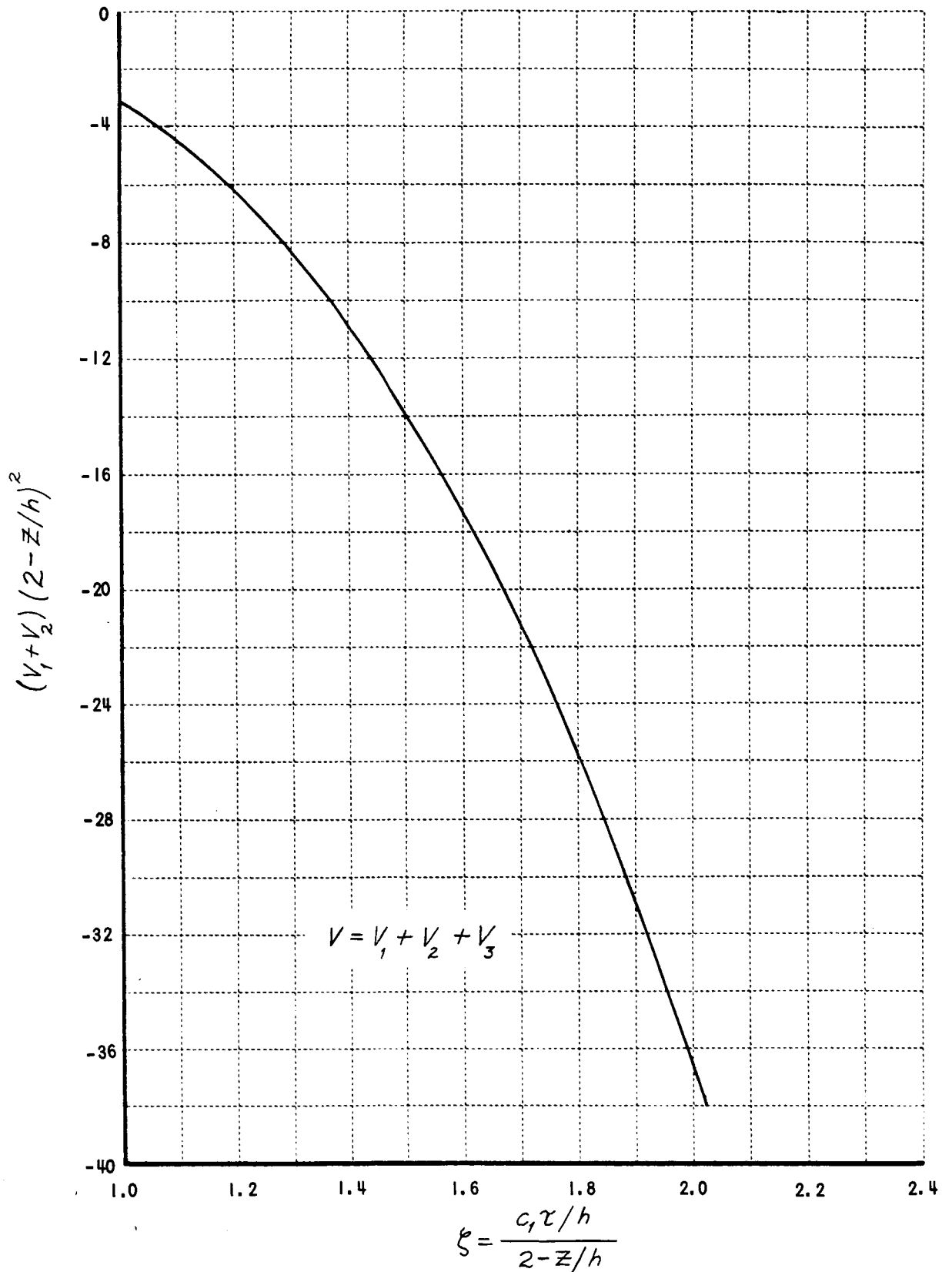
Figure 4 THE FUNCTIONS V_1 & V_2; $\nu = 1/4$
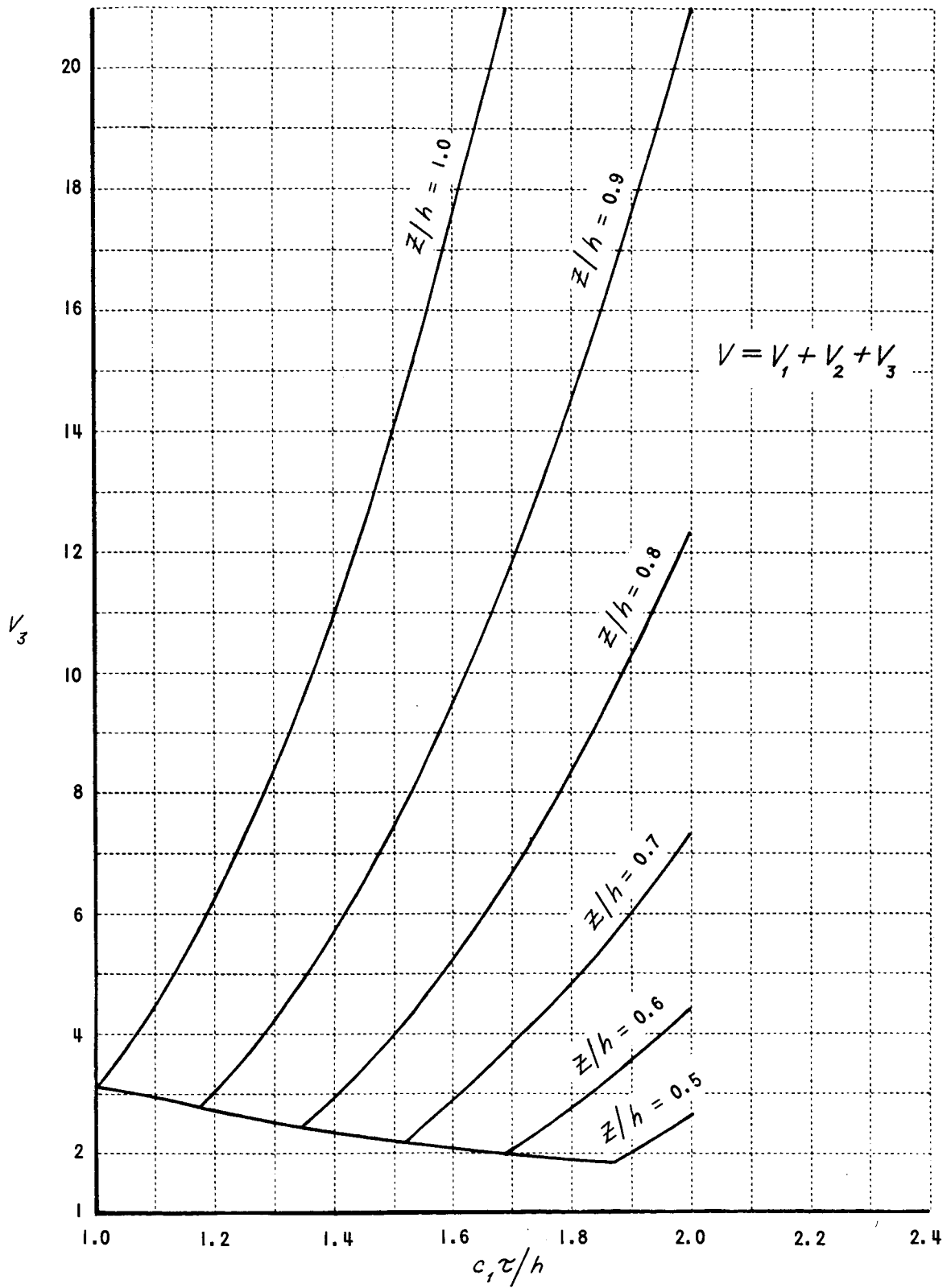
56   AI-1821-A-3

Figure 5 THE FUNCTION V_3 ; $\nu = 1/4$

The graph shows V_3 (vertical axis, ranging from 1 to 20) versus $c_1 \tau / h$ (horizontal axis, ranging from 1.0 to 2.4) with curves for $z/h = 1.0$, $z/h = 0.9$, $z/h = 0.8$, $z/h = 0.7$, $z/h = 0.6$, and $z/h = 0.5$.

$$V = V_1 + V_2 + V_3$$

Figure 6   THE FUNCTION $V = V_1 + V_2 + V_3$, $Z/h = 0.8$, $c_1 t/h = 1.5$, $\nu = 1/4$

AI-1821-A-3

Distribution List for
NASA CR-54250
CAL Report AI-1821-A-3

Advanced Research Projects Agency
The Pentagon
Washington, D. C. 20301
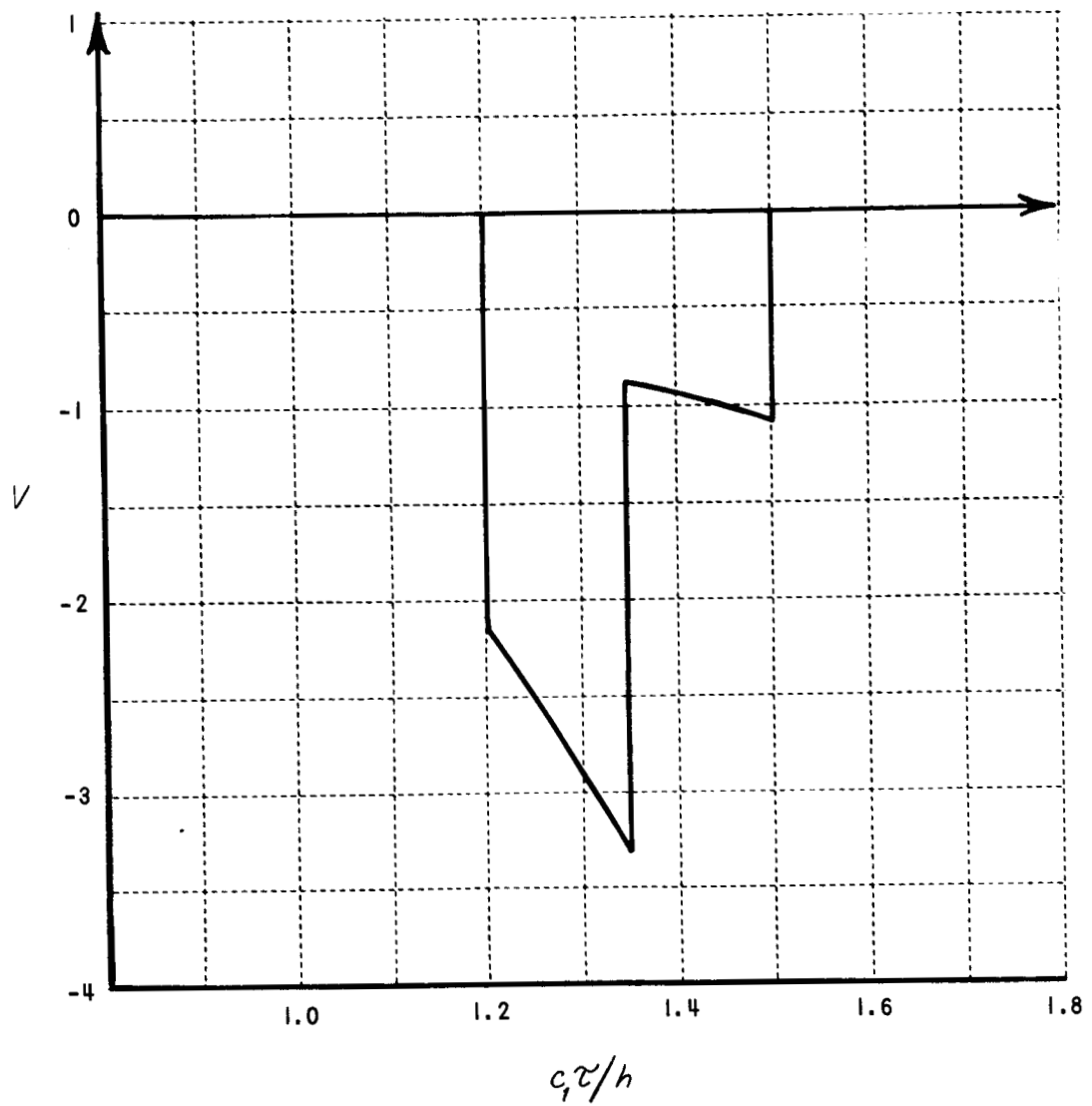Attn: John Huth (1)

Aerojet-General Corporation
1100 W. Hollyvale
Azusa, California
Attn: Paul I. Wood (1)

Aeronautical System Division (1)
Wright-Patterson AFB, Ohio

Aeronautical Systems Division
Wright-Patterson AFB, Ohio
Attn: Col. L. R. Standifer (1)

Aerospace Corporation
P. O. Box 95085
Los Angeles, California 90045
Attn: Jack H. Irving (1)
       Dr. Harold Mirels (1)

AiResearch Manufacturing Division
Phoenix, Arizona
Attn: E. A. Kovacevich (1)

Allis-Chalmers Manufacturing Company
P. O. Box 512
Milwaukee, Wisconsin 53201
Attn: Dr. Thomas P. Meloy (1)

ARO, Inc.
Arnold Air Force Station
Tennessee 37389
Attn: Dr. Clark H. Lewis (1)
       Dr. J. Lukasiewicz (1)

ASD (ASQWR)
Det. 4
Eglin Air Force Base, Florida
Attn: W. H. Dittrich (1)

U. S. Atomic Energy Commission
Germantown, Maryland
Attn: Lt. Col. G. M. Anderson (1)

     Col. E. Douthett, (1)
     SNAP-50/SPUR Project Office

     Herbert Rochen, (1)
     SNAP-50/SPUR Project Office

U. S. Atomic Energy Commission
P. O. Box 1102
Middletown, Connecticut
Attn: H. Pennington, (1)
     CANEL Project Office

U. S. Atomic Energy Commission (3)
Technical Information Service Extension
P. O. Box 62
Oak Ridge, Tennessee

Atomics International
P. O. Box 309
Canoga Park, California
Attn: Carl E. Johnson (1)

AVCO
Research and Advanced Development Division
201 Lowell Street
Wilmington, Massachusetts 01887
Attn: Librarian (1)
     Dr. R. G. Payton (1)

Ballistic Research Laboratories
Aberdeen Proving Ground
Maryland
Attn: Dr. F. E. Allison (1)
     Dr. F. D. Bennett (1)
     Dr. R. J. Eichelberger (1)
     Dr. J. T. Frasier (1)
     Dr. B. G. Karpov (1)
     J. H. Kineke (1)

Bell Telephone Laboratories
Whippany, New Jersey
Attn: Mr. Carl B. Loutzenheiser (1)
     Dr. Daniel Pope (1)

Boeing Corporation
Seattle 24, Washington
Attn: Jack Lundeberg (1)

Guggenheim Aeronautical Laboratory
California Institute of Technology
1201 East California Street
Pasadena, California
Attn: Prof. Julian D. Cole (1)
       Prof. Lester Lees (1)

Jet Propulsion Laboratory
California Institute of Technology
4800 Oak Grove Drive
Pasadena, California 91103
Attn: General Documents Control for
       Astronautics Information Abstracts (1)

Division of Geological Sciences
California Institute of Technology
Pasadena, California
Attn: Dr. C. H. Dix (1)

California Research Corporation
La Habra, California
Attn: Dr. F. G. Blake, Jr. (1)

Convair-Astronautics
5001 Kearny Villa Road
San Diego 11, California
Attn: Dr. Krafft A. Ehricke (1)

Graduate School of Aerospace Engineering
Cornell University
Ithaca, New York
Attn: Prof. E. L. Resler, Jr. (1)

Douglas Missile and Space Systems Division
Santa Monica, California
Attn: Dr. Martin Fiebig (1)
       Dr. John K. Wall (1)

Drexel Institute of Technology
32nd and Chestnut Street
Philadelphia 4, Pennsylvania
Attn: Dr. Pei Chi Chou (1)
       Dr. R. E. Llorens (1)

Electro-Optical Systems, Inc.
125 North Vinedo Avenue
Pasadena, California
Attn: Joseph Neustein (1)

Exotech, Inc.
Alexandria, Virginia
Attn: Dr. W. C. Cooley (1)

General Atomic
Division of General Dynamics Corporation
P. O. Box 608
San Diego, California
Attn: Dr. M. J. Nowak (1)
Dr. M. L. Scharff (1)
Dr. J. M. Walsh (1)

General Dynamics/Astronautics
P. O. Box 1128
San Diego, California 92112
Attn: Dr. J. J. Gilvarry, (1)
Mail Zone 596-00

General Electric Company
Flight Propulsion Laboratory
Cincinnati 15, Ohio
Attn: Morris A. Zipkin (1)

General Electric Company
Research Laboratory
P. O. Box 1088
Schenectady, New York 12301
Attn: Dr. Henry T. Nagamatsu (1)

General Electric Company
Missile and Space Division
Space Sciences Laboratory
Valley Forge Space Technology Center
P. O. Box 8555
Philadelphia 1, Pennsylvania
Attn: Edward Ray (1)
Mr. T. David Riney, (1)
Rm. M7023F

Defense Research Laboratories
General Motors Corporation
Box T
Santa Barbara, California
Attn: Dr. Jacques A. Charest (1)
Dr. A. C. Charters (1)
J. S. Curtis (1)
Dr. A. Q. Eschenroeder (1)
J. W. Gehring, (1)
Flight Physics Laboratory

Goodyear Aircraft Corporation
Akron, Ohio
Attn: Mr. S. J. Pipitone (1)

Harvard University
Cambridge, Massachusetts 02138
Attn: Dr. G. B. Benedek (1)

Illinois Institute of Technology Research Institute
10 West 35th Street
Chicago, Illinois 60616
Attn: Mr. D. C. Anderson (1)
      Dr. Thomas A. Zaker (1)
      Dr. F. J. Zimmerman (1)

Institute for Defense Analyses
400 Army-Navy Drive
Arlington, Virginia 22202
Attn: Librarian (1)
      Dr. F. B. Porzel (1)

Linden Laboratories
State College, Pennsylvania
Attn: Dr. Henry P. Kirchner (1)

Lockheed Missile and Space Company
P. O. Box 504
Sunnyvale, California
Attn: Charles Burrell (1)

Lockheed Aircraft Corporation
Missile Systems Division
Palo Alto, California
Attn: Hal H. Greenfield (1)

Arthur D. Little, Inc.
Cambridge 40, Massachusetts
Attn: Librarian (1)

Arthur D. Little, Inc.
30 Memorial Drive
Cambridge 42, Massachusetts
Attn: N. Wiederhorn (1)

Los Alamos Scientific Laboratory
P. O. Box 1663
Los Alamos, New Mexico 87544
Attn: Dr. Melvin H. Rice (1)

M. B. Associates
1279 Boulevard Way
Walnut Creek, California
Attn: Dr. D. Sawle (1)

The Martin Company
Baltimore, Maryland 21203
Attn: Dr. Joseph Sternberg, (1)
    Space Systems Division, Mail No. 390

McGill University
McDonald Engineering Building
Montreal, Canada
Attn: G. V. Bull (1)

National Aeronautics and Space Administration
Ames Research Center
Moffett Field, California 94035
Attn: Librarian (1)
    D. E. Gault (1)
    C. R. Nysmith (1)
    J. Summers (1)

National Aeronautics and Space Administration
Scientific and Technical Information Facility
Box 5700
Bethesda 14, Maryland
Attn: NASA Representative (1)

National Aeronautics and Space Administration
Goddard Space Flight Center
Greenbelt, Maryland 20771
Attn: Merle Alexander (1)
    Milton Schech (1)

National Aeronautics and Space Administration
Jet Propulsion Laboratories
California Institute of Technology
4800 Oak Grove Drive
Pasadena, California
Attn: John Paulson (2)

National Aeronautics and Space Administration
Langley Research Center
Langley Station
Hampton, Virginia 23365
Attn: Librarian (1)

National Aeronautics and Space Administration
Lewis Research Center
21000 Brookpark Road
Cleveland, Ohio 44135
Attn: D. Besnatowicz (1)
    R. Denington (1)
    John E. Dilley, (1)
    Contracting Officer, MS 86-1

National Aeronautics and Space Administration
Lewis Research Center
21000 Brookpark Road
Cleveland, Ohio 44135
Attn: J. B. Esgar (1)
      John J. Fackler (SPSPS) (1)
      Mr. G. Goldberg (1)
      M. Gutstein (3)
      Seymour Lieblein, (2)
      Fluid Systems Components Division
      I. J. Loeffler (1)
      B. Lubarsky, (1)
      Space Power Systems Division
      George Mandel, (1)
      Librarian
      Roger Mather (1)
      Norman T. Musial (Patent Counsel) (1)
      Henry O. Slone, (1)
      SNAP-8 Branch
      Gordon T. Smith (1)
      F. S. Stepka (1)

National Aeronautics and Space Administration
Manned Spacecraft Center
Houston 1, Texas
Attn: Librarian (1)
      Paige Burbank (1)

National Aeronautics and Space Administration
Marshall Space Flight Center
Huntsville, Alabama 35812
Attn: Dr. E. D. Geissler (1)
      Dr. O. K. Hudson (1)
      W. Johnson (1)
      W. D. Murphree (1)
      Russell H. Shelton (1)
      Dr. Ernst Stuhlinger (1)

National Aeronautics and Space Administration
600 Independence Avenue SW
Washington, D. C. 20546
Attn: Dr. R. L. Bisplinghoff (1)
      M. T. Charak (1)
      C. T. D'Aiutolo (1)
      J. W. Keller (1)
      James J. Lynch (RN) (1)

National Aeronautics and Space Administration
Office of Scientific and Technical Information
Washington, D. C.
Attn: AFSS-A (1)

AI-1821-A-3

National Aeronautics and Space Administration
Western Operations Office
150 Pico Boulevard
Santa Monica, California
Attn: John Keeler (1)

U. S. Naval Ordnance Laboratory
White Oak, Silver Spring, Maryland 20910
Attn: V. C. D. Dawson (1)
      Dr. J. W. Enig (1)
      Eva Lieberman, Librarian (1)
      R. K. Lobb (1)
      R. Piacesi (1)
      A. E. Seigel (1)

Naval Research Laboratory
Washington, D. C.
Attn: W. W. Atkins (1)
      Mrs. Katherine H. Cass, (1)
      Code 1572
      S. M. Halperson (1)
      Dr. H. Marcus, (1)
      Mechanics Division

North American Aviation, Inc.
Los Angeles 45, California
Attn: Advanced Electrical Projects (1)

North American Aviation, Inc.
Space and Information Systems Division
12214 Lakewood Avenue
Downey, California 90241
Attn: Mr. C. A. Papp (1)

Oak Ridge National Laboratory
Oak Ridge, Tennessee
Attn: W. D. Manly (1)

Office of Naval Research
Department of the Navy, Code 735
Washington, D. C. 20360
Attn: E. E. Sullivan (1)
For: Code 429

Pennsylvania State University
State College, Pennsylvania
Attn: Dr. H. H. Calvit (1)
      Prof. N. Davids (1)

Physics International, Inc.
2229 Fourth Street
Berkeley 10, California
Attn: Mr. Jere G. Harlan (1)

Pratt & Whitney Aircraft
East Hartford, Connecticut
Attn: William H. Pedolny (1)

The RAND Corporation
1700 Main Street
Santa Monica, California 90406
Attn: Dr. Harold Brode (1)
      F. R. Collbolm (1)

Republic Aviation Corporation
Farmingdale, Long Island, New York
Attn: Dr. William McIlroy, (1)
      Power Conversion System Division

Sandia Corporation
Sandia Base
Albuquerque, New Mexico
Attn: Mr. R. C. Bass (1)
      Dr. W. Herrmann (1)

Shock Hydrodynamics Inc.
Sherman Oaks, California
Attn: Dr. R. L. Bjork (1)

Space Technology Laboratories, Inc.
P. O. Box 95001
Los Angeles 45, California
Attn: George E. Mueller (1)

TRW, Space Technology Laboratories
One Space Park
Redondo Beach, California
Attn: Dr. Saul Altshuler (1)

Stanford Research Institute
333 Ravenswood Road
Menlo Park, California
Attn: Dr. D. R. Curran (1)

Stanford University
Stanford, California 94305
Attn: Prof. M. D. VanDyke, (1)
      Dept. Aeronautics & Astronautics

AI-1821-A-3

State University of New York at Buffalo
Division of Interdisciplinary Studies
Buffalo, New York 14214
Attn: Dr. David Benenson (1)
      Prof. I. H. Shames (1)

Technik, Inc.
50 Jericho Turnpike
Jericho, New York
Attn: Mr. Paul Marnell (1)

Tech/Ops, Inc.
Burlington, Massachusetts
Attn: V. E. Scherrer (1)

Tennessee Polytechnic Institute
Cookeville, Tennessee
Attn: Prof. R. Kinslow (1)

Therm Advanced Research, Inc. (1)
100 Hudson Circle
Ithaca, New York

Thompson Ramo Wooldridge, Inc.
New Devices Laboratory
7209 Platt Avenue
Cleveland 4, Ohio
Attn: Librarian (1)

University of California
Berkeley, California 94720
Attn: Prof. Werner Goldsmith (1)

University of California
Los Angeles, California 90024
Attn: Prof. N. Rott, (1)
      Dept. of Engineering

University of California
Lawrence Radiation Laboratory
P. O. Box 808
Livermore, California
Attn: Dr. Russell E. Duff (1)

University of Oklahoma
Norman, Oklahoma
Attn: Dr. F. C. Todd (1)

University of Rochester
Rochester, New York
Attn: Dr. Robert G. Loewy, (1)
      Dept. Mech. & Aerospace Sci.

AI-1821-A-3

Institute for Aerospace Studies
University of Toronto
Toronto, Ontario, Canada
Attn: Dr. I. Glass (1)

United Electro Dynamics, Inc.
Pasadena, California
Dr. E. A. Flinn (1)

Utah Research and Development Corporation
1820 South Industrial Road
Salt Lake City, Utah 84014
Attn: Dr. E. Cannon (1)

Westinghouse Electric Corporation
Astronuclear Laboratory
P. O. Box 10864
Pittsburgh 36, Pennsylvania
Attn: Library (1)

Materials Laboratory
Physics Division
Wright Field, Ohio
Attn: Mr. Alan K. Hopkins (1)

AI-1821-A-3